TriDurLE

National Center for Transportation Infrastructure Durability & Life-Extension

Project ID: 2020-FAU-02

Corrosion propagation monitoring using galvanostatic pulse on reinforced concrete legacy samples

Final Report

By

Francisco J. Presuel-Moreno
with
K. Hoque, A. Rosa-Pagan

for

National University Transportation Center TriDurLE
Department of Civil & Environmental Engineering
405 Spokane Street PO Box 642910
Washington State University Pullman, WA 99164-2910

January 2022

Acknowledgements

The author is indebted to the USDOT and TriDurLE for financial support, FDOT for matching support. The author also thanks FDOT State Materials Office (SMO) for assisting in preparing the legacy reinforced concrete samples. The author also acknowledges the assistance of several students who worked as graduate/undergraduate research assistants at FAU–SeaTech marine materials and corrosion lab during the duration of this project (A. Rosa-Pagan, K. N. Hoque, A. Ibarra) and during the previous phase (R. Bencosme, M. Nazim, K. Hoque).

Disclaimer

The opinions, findings, and conclusions expressed in this publication are those of the author and not necessarily those of the State of Florida Department of Transportation, nor the United States Department of Transportation.

Table of Contents

Contents

List of Figures

List of Tables

Executive Summary

Legacy samples were monitored. Outdoor exposed legacy samples were prepared in 1994 and have been subjected to wet/dry cycles with seawater during the wet part of the cycle. Two sets of samples were stored indoors: single rebar and three rebar specimens, these samples were prepared in 2016 and were subjected to accelerated chloride transport via a migration method at least two months after casting. The concrete composition of these samples was binary or ternary (see details in the body of the report). The indoor samples have various lengths of solution reservoir and the samples are stored in plastic bins that allow the moisture surrounding the specimens to remain above 80% RH. Although the notice to proceed was received August 2020, this report includes measurements performed February 2020 to August 2021 for the indoor samples, and August 2020 to August 2021 for the outdoor samples.

Electrochemical measurements were performed using galvanostatic pulse method to monitor the legacy samples. The applied pulse current magnitude was initially 10 μA, but it was adjusted to either a smaller or lager magnitude depending on how much the rebar was polarized with the current on. Initially an anodic current was applied, but it was decided to change it to a cathodic current to minimize activation due to the galvanostatic pulse. Each measurement allowed to identify the rebar instantaneous open circuit potential (OCP), solution resistance (Rs), and polarization resistance (Rc). It was assumed that all rebars were corroding and the Icorr was calculated assuming a B constat of 26.1 mV (in the Stern-Geary equation). Ecorr vs. Icorr and Icorr vs. Rs correlations were prepared using three most recent measurements (i.e., with measurements made between April and August 2021). The findings of the Ecorr vs. Icorr correlations suggest that the slope is not the same for all sample groups, but they appear to confirm that all rebars are in an active state. It was observed that the Ecorr-Icorr value pairs of some rebars suggest less active state and deviate somewhat from the average slope. This observation is more pronounced on some outdoor samples that those exposed indoors. An interesting observation from the Icorr vs. Rs correlation corresponding to outdoor samples is that some rebars showed significantly smaller Rs with relative large Icorr values, these appear to correspond to rebars that now show cracks above the rebar.

Chapter 1. Introduction

1.1 Problem Statement

Although there have been several studies regarding the corrosion propagation, these studies typically consist of samples in which chlorides are added to the concrete. Then in most cases a current is applied to accelerate the corrosion. The samples after some time present cracks and shortly after the samples are forensically analyzed. One concern is that the corrosion could evolve in a manner different that what takes place in the field.

Recent reviews have acknowledged the effect of sample size, sample geometry, exposure method on the amount of chlorides that cause corrosion of the reinforcing steel to initiate[1]. There are some reports [2-3] that indicate that the chloride threshold is lower on concrete with supplementary cementitious materials, particularly for concrete with high fly ash content (i.e., ≥50%); thus, this needs to be considered when modeling service life. There are several reports[4-5] that indicate that the corrosion rate of carbon steel rebar embedded in high performance concrete is lower (at the early stages) when compared to rebar corroding on concrete with no supplementary cementitious materials. This observation in part can be attributed to the higher concrete electrical resistivity for concrete with supplementary cementitious materials (vs. concrete with no cm) when comparing concretes with similar moisture content (smaller macrocell effects). The higher resistivity is in part due to pore refinement and higher tortuosity that develops with time for those concretes with supplementary cementitious materials. However, as corrosion progresses and causes damage on the concrete; the apparent concrete resistivity (or solution resistance) of moist cracked concrete can become small, and this could allow corrosion rate to occur at a higher rate even on rebars embedded in high performance concrete.

It is important to note that the concrete electrical resistivity could also increase significantly if the concrete is exposed to dry conditions (low relative humidity). Thus, it is important to be aware of the exposure conditions. For structures that are partially immersed, as are many bridges exposed in Florida, the moisture condition is high all year round, due to the high humidity prevalent most of the year. Most of the reported corrosion rate values correspond to values obtained shortly after corrosion initiation. As mentioned above, as the chloride concentration increases at the rebar trace, the corrosion rate of carbon steel also tends to increase. As time passes, the corroding area will tend to increase (either the corroding site becomes larger or corrosion initiates at additional locations). The corroding sites then produce corrosion products that build up with time. A high moisture content of the pore structure can allow the corrosion products to be transported thru the pore structure (saturated concrete), or if partially filled with pore solution the corrosion products (once built-up has occurred) apply tensile stress that then can eventually cause cracks. The rebar cross-section loss can in some cases be large (after corrosion propagation has taken place for some time). Thus, monitoring the corrosion rate for a longer period within the propagation stage is relevant under various exposure conditions. Legacy (samples prepared as part of previous projects) samples are available at FAU[6] in which corrosion propagation can be investigated and monitored.

This study is aimed to better understand how corrosion propagates on rebars embedded on concrete with supplementary cementitious materials, via legacy samples. Legacy samples were monitored as part of this project. There are indoor and outdoor exposed legacy samples. The outdoor exposed samples were

prepared in 1994 with low w/cm and there are both OPC samples and binary mixes (see description in the experimental section). These samples were monitored several times using galvanostatic pulse measurements. The Icorr vs. time during the monitored period are reported in the results section. Several samples either had cracks or developed cracks during the monitored period.

Legacy indoor samples prepared in 2016, were also monitored as part of this project. These samples were prepared with binary or ternary concrete compositions. Samples were prepared with a single rebar and other samples were prepared with three rebars. The experimental section describes the details. Chloride transport was accelerated by applying an electric field a few months after the samples were prepared. Thus, the passive layer was allowed to form on the rebar surface of the embedded rebar. The results section includes plots of Icorr vs. time and Ecorr vs. time for selected samples (the appendix includes results of the other monitored samples). The cumulative mass loss using available Icorr values (obtained using GP measurements) were calculated.

1.2 Objectives

The objectives are twofold: (1) Identify the effects of moisture content on the corrosion propagation in the reinforced concrete; (2) Evaluate the degree of corrosion within the reinforced concrete correlating parameters obtained from galvanostatic pulse (GP) measurements: OCP, corrosion current (Icorr), solution resistance (Rs). One of the parameters monitored via the GP method is the corrosion current as the corroding area is not known. Mass loss will be estimated using Faraday's law (for indoor specimens only), the estimated mass loss will include Icorr values obtained previously (2017 to 2020).

1.3 Expected Contributions

Plots correlating Icorr vs. Rs and Ecorr (OCP) vs. Icorr for the different sample groups have been prepared. These plots were prepared using recent set of measurements (at least three values taken during the last five months of monitoring). These correlations will add to those available in the literature.

1.4 Report Overview

The report presents a brief literature review, then the methodology chapter is presented (note that additional details on the experimental can be found on a previously published report [Ref]). The results section presents typical results of the monitored parameters, but most emphasis is on the Icorr vs. time. An appendix contains Icorr vs. time for most of the rebars monitored as part of the current effort. The discussion section presents the correlations prepared for both outdoor and indoor results and for rebars embedded in indoor specimens the estimated mass loss is presented. No signs of cracks are visible on the indoor samples (although rust spots are now visible above very few rebars), cracks are visible above the rebar on several outdoor specimens. Year 2 will include the forensic analysis of selected outdoor specimens.

Chapter 2. Literature Review

Once corrosion of the reinforcing steel has initiated in atmospherically exposed reinforced concrete, its propagation is controlled primarily by the supply of oxygen, moisture content and resistivity of concrete [7]. The length of the corrosion propagation stage is the time from corrosion initiation to a defined limit state. There are several damage indicators associated with different limit states such as loss of rebar cross-sectional area, loss of bond strength between steel and concrete and corrosion-induced concrete cover cracking [8]. Corrosion of the reinforcing steel causes an initial increase in rebar to concrete bond strength due to the increased rebar surface roughness but further corrosion results in loss in bond strength. The consequent corrosion-induced cracking tends to reduce the confining capacity of surrounding concrete.

Several researchers have considered the appearance of corrosion induced surface cracks as a performance limit state as it is relatively easy to determine in a corroding reinforced concrete structure [9,10]. Concrete cover cracking is caused by the accumulation of expansive corrosion products at the steel-concrete interface when these exceed the critical penetration depth (X_{crit}). Generally, corrosion products can have a volume up to four to six times greater than that of the original steel [11]. However, Hansson et al. found that the volume of corrosion products observed in concrete is between 2.2 and 3.3 times greater than that of steel from which they formed [12].

Most rebar corrosion propagation studies assume corrosion around the whole rebar circumference, and along most of the rebar (with a few exceptions). As corrosion progresses, the corrosion products continue to accumulate and once it fills up the concrete pores, radial and hoop stresses start to develop. Cover cracking begins when the stress state satisfies a certain cracking failure criterion. The degree of moisture could dictate the type of corrosion products that are present and how far the products move through the pore structure.

The aggressive nature of chloride-induced corrosion and the related rate of deterioration of reinforced concrete structure are worsened due to the presence of cracks in concrete (cracks are sometimes due reasons other than corrosion of the reinforcing steel.). Cracks impair the durability of reinforced concrete structures by creating preferential paths for the penetration of corrosion-inducing species leading to relatively earlier initiation and faster propagation of steel corrosion and consequently a reduction in service life. The depth, thickness and origin of the cracks affect when corrosion initiates and how it propagates. [8] If no cracks are present, both the initiation and propagation phases are usually a function of, among other factors, the penetrability of the concrete cover, the cover thickness, resistivity of concrete, and the corrosion resistance of the steel bars [13-15]. In the presence of cracks, several studies have shown that the factors affecting corrosion rate in uncracked concrete are still relevant, but their effects(relevance) is significantly reduced. The effects of cracks on corrosion vary not only with their width, but also with depth, frequency, orientation (relative to the steel reinforcement), self-healing potential of the concrete, and activity or dormancy.

Melchers and Chaves [16] proposed that chloride concentrations are involved only indirectly in initiating reinforcement corrosion and in serious active corrosion. According to Melchers and Chaves[16], the primary role of chlorides in chloride-induced damaging corrosion of reinforcement lies in accelerating the solubility of the alkaline calcium hydroxide in the concrete matrix, including around

the reinforcing bars and thereby allowing depassivation of the steel reinforcement. The dissolution of alkalis is increased for the more permeable concretes as these have higher internal surface areas for alkali dissolution. This view provides an understanding that longer durability can be achieved through use of more dense, low permeability concretes. Melchers and Chaves also mentioned that high concrete alkalinity can be achieved by using limestone or non-reactive dolomites as concrete aggregates.

Several research efforts over the last few decades have been focused on developing models that can estimate time to cracking. Most of these studies were focused on OPC concrete without admixtures; very few models have been done that include high performance admixtures. Jamali et al. [17] reviewed empirical, analytical, and numerical models which have been developed for modeling corrosion-induced concrete cover cracking due to reinforcing steel corrosion. Jamali mentioned that the parameters need to be considered are corrosion rate, type of corrosion products, corrosion accommodating region, mechanical properties of materials and geometry. When the corrosion morphology is due to the localized corrosion (as per chloride-induced corrosion), the anodes and cathodes could be separated, and corrosion products form only locally. These results in changing the geometrical locations of the corrosion products and thus affects when and where cracking occurs.

According to Otieno et al. [18] chloride-induced corrosion is accelerated by cracks with increase in penetrability. It is observed that with a given type of binder and w/b ratio, corrosion rate increases with increase in crack width whereas for a specific crack width, corrosion rate increases with decrease in concrete quality. When concrete structures are exposed to chlorides, cracks have a severe effect which increases penetrability of concrete and hence corrosion occurs at higher rates.

Otieno et al. [19] assessed the effect of drying duration and concrete quality on corrosion rates of steel in accelerated corrosion tests in the laboratory. The results showed that the duration of drying affects corrosion rate of steel in concrete, having the wetting duration kept constant; however, the combined effects of concrete quality and drying duration need to be considered. Denser, less penetrable concretes with low w/b ratios were less influenced by the drying duration, with the opposite being true for less dense, more penetrable microstructure concretes with higher w/b ratios. It has been shown that the denser microstructure concretes with high resistivity exhibited resistivity corrosion control while the less dense microstructure ones with low resistivity exhibited both cathodic and resistivity corrosion controls.

Torres-Acosta [10] and Busba [20] mentioned in their experiments and empirical model the effect of anode-length and how the average penetration depth increased with cover/diameter (of rebar) increase for a constant c/L (concrete cover/anode length). Torres-Acosta [10] and Busba [20] experiments ensured that corrosion was taking place around the whole perimeter of the rebar (with different length). Otieno et al. [8] did a review of the corrosion rates that have been used and include results of experiments with an incipient crack. Angst et al. [21] described the effect of reinforcement length (sample size) on the chloride threshold.

Jamali et al. [17] described that in some cases where chloride-induced corrosion took place rust-stains or cracks were invisible; but, upon forensic examination, a significant cross-sectional loss was found at the corroding site. Angst et al. [22] described, as an example, a bridge deck with a damaged waterproofing membrane, where concrete is locally saturated with water and hence oxygen starvation is likely. In such instances, anodic iron dissolution could occur (once corrosion has initiated) without enough precipitation of corrosion products to form cracks [23]. This type of corrosion is usually referred to as

‘black rust’ [23] since the iron may remain dissolved in the concrete pore solution until the concrete is removed during visual inspection and thus access to oxygen is provided. Walsh and Sagüés [24] reported similar results by performing forensic analysis of reinforced concrete pile that was fully immersed for an extended time period.

In addition, Walsh and Sagüés [24] and Sanchez and Sagüés [25] mentioned a halo effect (cathodic prevention similar to was first reported for pitting corrosion of stainless steel by Budiansky [26]) of a corroding site on the surrounding steel, such that the next corroding site was located at a certain distance from the initial anode.

In partially-immersed reinforced concrete bridges expose to a marine environment, the chloride ions penetrate from the surface toward the reinforcement. As a result, the side of the rebar facing the chloride exposed concrete surface reaches the chloride threshold first and then corrode. The initial corrosion site can be as small as a small pit (e.g., <1 mm diameter). Once corrosion has initiated, it is likely that the corroding site would exert some cathodic prevention on the surrounding steel area such that the next corroding site would be located some distance from the initial corroding site. Its throwing power will depend on the concrete resistivity and moisture content to mention two contributing factors.

It has been reported that the corrosion products are more soluble in the presence of chlorides, high moisture might also enhance how far these corrosion products can travel through the concrete microstructure (e.g., at tidal and submerged region elevations) [27]. On the other hand, when chloride concentration is quite high (significantly larger than the chloride threshold), corrosion might then occur around the whole rebar, having a considerable anode length, which then could proceed as often modeled and cause cracking and eventually spalling.

There have been a few efforts of investigating the effects of corrosion on the mechanical performance of rebars and there are s few studies showing the long-term progression of corrosion on mechanical properties. As part of this review, a few studies were found that focus their efforts on chosen levels of corrosion only. These studies also focus on investigating the effects of the independent variables of mass loss due to corrosion and rebar diameter have on the mechanical properties of the rebar but do not consider the effect other variables may have on corrosion rate and the mechanical properties of the corroding rebar such as concrete composition, lengths of the corroding site.

Three recent research papers [28-30] present both mathematical models and experiments performed to develop relationship equations between rebar mass loss due to corrosion and mechanical properties of the rebar. Imperatore [29] study used the data from experiments with artificially induced corrosion samples to develop equations which relate mass loss to stress and ductility of the reinforcement. Imperatore [29] experiments were done for uniform corrosion. Moreno et al.[30], developed the relationships to tensile strengths using a multivariable regression approach establishing the independent variables as mass loss percentage and diameter. Moreno [30] also used artificially induced corrosion samples with the difference that the rebars showed pitting corrosion. Vanama [28] study expanded on Imperatore’s and Moreno’s work and that of others and developed equations that can be used for uniform and localized corrosion, but might only be valid within the reported ranges for mass loss. Vanama use both naturally and artificially induce corrosion specimens. Vamana [28] study reports on two groups of samples: naturally induced corrosion believed to be due to carbonation and artificially induced corrosion due to chlorides and accelerated. Vamana’s study included rebars that experienced as

much as 60% mass loss. A recent MS thesis contains a more in depth review of these three papers [31]. Rosa-Pagan used the estimated mass loss using the Icorr results of the three rebar legacy samples and Vamana study to estimate current reduction in mechanical properties (but values were not within the mass loss range reported by Vamana, because of this the findings are not included in here and the reader is referred to the thesis)

Chapter 3. Methodology

Outdoor Specimens

Figure 1 shows the dimensions of the 5 rebar specimens exposed outdoors at FAU-SeaTech in Dania Beach, FL. These samples were prepared in 1994, Appendix A contains tables describing the concrete mix compositions for the specimens. All samples were prepared with low w/cm, target w/cm of 0.37 was used. Prior to outdoor exposure testing (shortly after casting), the specimens were inverted (as–cast face down); and a plastic pond was mounted on what became the top surface (see Figure 1). The exposure took place outdoors most of the time, but early on the specimens were exposed indoors for a couple of years. A one week wet — one–week dry ponding cycle was instituted in January 1995 using fresh natural sea water. The typical conductivity of seawater measured at the FAU site is ~ 35 mS/cm. As shown in Figure 1, each of the bottom bars was electrically connected to one of the top bars so that a macrocell resulted between the two. These connections stop working around 2018. The wet and dry cycles were suspended from June 2018 to June 2020. For the approx. 400 days reported in here the samples were subjected to wet and dry cycles with seawater. Typically, the samples were with seawater for two weeks with and two weeks without. Galvnostatic Pulse measurements were performed on the top row rebars at least once every other month. There are 30 outdoor samples remaining, with several samples having only two rebars left on the top row and one sample with only one. Out of the 30 samples 25 are of known composition with the remaining five the composition is not known, other than the w/cm was still 0.37.

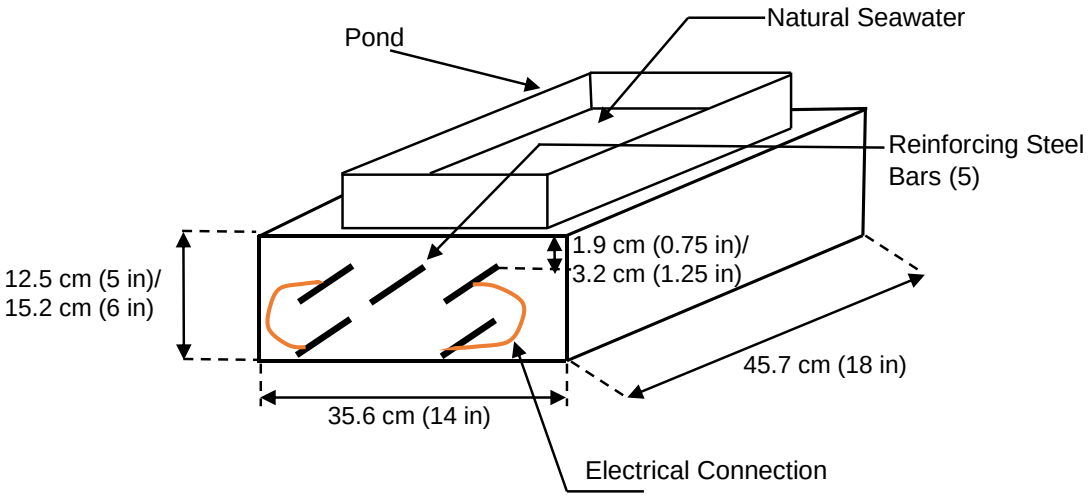

Figure 1. Five-rebar specimen diagram (outdoor specimens)

Indoor exposed legacy samples (Single and Three rebar specimens)

The legacy indoor exposed samples were prepared during spring 2016 and summer 2016. Samples with four different compositions were prepared, see Table 1 for the compositions. Three concrete mixes were prepared with a w/cm ratio of 0.41 and one mix was prepared with a w/cm of 0.37. The SL specimens were prepared with blast furnace slag (50% cement replacement); FA specimens with Fly Ash (20% cement replacement); Mix T1 contains both FA and blast furnace slag, and mix T2 contains both FA and silica fume. Additional details of each concrete mix can be found in Appendix 2 of Ref [Report]. Single and three rebar specimens were prepared. The three rebar specimens are 30.5 cm × 30.5 cm × 7.6 cm (12

× 12 × 3 in) and contain #4 rebars. The rebars were equally spaced with 2.5 cm (1 inch) concrete cover measured from the mold bottom surface (this became the top surface during exposure). The dimensions for the single rebar samples are 30.5 cm × 10.1 cm × 6.9 cm, the rebars are #3. Four series of samples were prepared two with binary composition and two with ternary composition.

Table 1. Concrete mix detail for specimens prepared Spring and Summer 2016

Mix	Cast Date	Cementitious Content	Cement Content	20% FA	8%SF	50% Slag	Fine agg.	Coarse agg.	w/cm ratio
		(kg/m^3)	(kg/m^3)	(kg/m^3)	(kg/m^3)	(kg/m^3)	(kg/m^3)	(kg/m^3)	
SL	4/4/2016	390	195		0	195	782	1009	0.41
FA	4/18/2016	390	312	78	0	0	967	833	0.41
T1	8/19/2016	390	117.5	78.3	0	195.18	761	1009	0.41
T2	8/19/2016	390	289	70	31	0	790	1046	0.37

Single and three rebar specimens were prepared. The three rebar specimens are 30.5 cm × 30.5 cm × 7.6 cm (12 × 12 × 3 in) and contain #4 rebars. The rebars were equally spaced with 2.5 cm (1 inch) concrete cover measured from the mold bottom surface (this became the top surface during exposure). The dimensions for the single rebar samples are 30.5 cm × 10.1 cm × 6.9 cm, the rebars are #3. Four series of samples were prepared two with binary composition and two with ternary composition. Table 1 presents the nominal compositions. Table 2 shows how many samples per each geometry and composition were available. A solution reservoir of varying length was installed on each sample on the bottom mold surface, Table 3 and Table 4 list the sample ID with the reservoir length for single and three rebars specimens respectively. All samples had stainless steel mesh or a TiMMO mesh embedded on the top surface at casting (bottom surface during exposure). All samples were exposed in containers that held calcium hydroxide solution, the reservoir was filled with 10 wt% NaCl solution. Electromigration was used to accelerate the transport of the chlorides into the concrete (Refs [] describe in detail how this was done and how many Ampere-hour were applied to each sample), this process took place over several months. By early 2017, the electromigration was suspended and the samples were monitored using electrochemical techniques. Refer to FDOT report [Ref] for early monitoring. As part of this project, the monitoring was resumed. The samples remain exposed in high humidity environment, but the solution was periodically removed for at least a couple of weeks. This was done to allow O_2 to replenish and reach the rebar depth.

Table 2. Number of samples available

	Specimen type	
	Single Rebar	Three Rebar
SL	9	11*
FA	9	12
T1	4	4
T2	5	4

Table 3. Sample ID and corresponding reservoir length (single rebar specimens)

Sample ID	Reservoir Length (cm)	Sample ID	Reservoir Length (cm)	Sample ID	Reservoir Length in (cm)
SL-1	17.5	FA-1	5	T1-6	15
SL-2	17.5	FA-2	5	T1-7	5
SL-3	17.5	FA-3	5	T1-8	15
SL-4	2.5	FA-4	7.5	T1(9)	10
SL-5	2.5	FA-5	7.5	T1(10)	5
SL-6	5	FA-6	7.5	T2-1	5
SL-7	5	FA-7	17.5	T2-2	15
SL-8	5	FA-8	17.5	T2-3	5
SL-9	10	FA-9	17.5	T2-4	10
SL-10	10	FA-10	2.5	T2-5	5
SL-11	10	FA-11	2.5	T2-11	15

Table 4. Sample ID and corresponding reservoir length (three rebar specimens)

ID	Composition	Reservoir Length (cm)	ID	Composition	Reservoir Length (cm)
1X	SL	5	17X	SL	5
2X	SL	2.5	18X	FA	15
3X	SL	10	19X	SL	2.5
4X	SL	15	20X	FA	10
5X	FA	2.5	21X	FA	10
6X	SL	10	22X	SL	15
7X	FA	5	23X	FA	5
8X	SL	10	24X	FA	15
9X	SL	3	25X	T1	5
10X	FA	2.5	26X	T1	2.5
11X	FA	2.5	27X	T1(27X)	10
12X	FA	5	28X	T1(28X)	5
13X	FA	10	29X	T2(29X)	10
14X	FA	15	30X	T2(30X)	2.5
15X	SL	10	31X	T2(31X)	5
16X	SL	5	32X	T2(32X)	5

Samples placed in the Environmental chamber

A number of the single rebar samples as well as three rebar samples were selected and transferred to an environmental chamber on 2/7/2020. Samples were selected by comparing recent Ecorr and Icorr values. For each concrete composition (SL, FA, T1, and T2), two single rebar specimens and one three rebar specimen were selected. Before transferring to the environmental chamber, the weight and Ecorr values of these specimens were recorded for later comparison. Table 5 lists different single rebar and three

rebar samples that were transferred to the environmental chamber.

Initially, all these specimens were kept in the environmental chamber at a temperature of 35ºC and 30% RH. After 14 days, the selected samples condition was changed to a high humidity environment (a temperature of 27ºC and 85% RH). Electrochemical measurement (GP) was carried out at least once a week (first four weeks back with high moisture) on these specimens starting from 2/21/2020, and then at least once in every two months. From GP measurement; OCP or Ecorr, Rs, Rc, and Icorr values were collected. Later, the humidity in the environmental chamber was increased to about 92% RH on 3/17/2020, in order to improve internal moisture in the concrete of the selected specimens. The period reported in here is from February 2020 to August 2021.

Table 5: Different single rebar and three rebar samples transferred to the environmental chamber according to the reservoir length

Concrete Mix	Mesh Length (cm)	Sample Name
SL	5	SL-7
	5	SL-8
	10	15X
FA	7.5	FA-4
	7.5	FA-6
	10	21X
T1	5	T1-7
	10	T1-9
	10	27X
T2	15	T2-2
	5	T2-3
	10	29X

GP measurements.

Galvanostatic Pulse (GP) method was used to monitor both indoor and outdoor samples. The duration of the pulse was 150 seconds (sometimes it was run up to 200 seconds), and the base amount of applied current was 10 μA (this value was adjusted to keep the rebar with the pulse on within a potential range of 4 to 25 mV). The current was initially anodic, but starting April/May 2020 a cathodic current is being applied . The GP test measures the open circuit potential for a few seconds first (OCP or Ecorr). Then the pulse is applied and the rebar potential as a function of time is measured every 0.2 seconds. The solution resistance (R_s) is calculated by using the rebar potential prior to the current pulse and using the first potential reading with the current pulse (i.e., the initial on–potential recorded). The R_c value was calculated by obtaining the difference between the initial on–potential and last potential value measured with the pulse on. The I_{corr} was calculated using the R_c values and a B constant of 26.1 mV. For samples in the environmental chamber the reported period is from February 2020 to August 2021, for the rest of the indoor samples the reported period is form June 2020 to August 2021, and for the outdoor samples the reported period is from August 2020 to August 2021.

Chapter 4. Results and Discussion

Indoor Samples

Single Rebar SL samples.

The largest Icorr was observed on rebars embedded in samples with 10 cm solution reservoir and reached values as high as 30 μA, the most recent Icorr ranges between 10 and 15 μA. Figure 2 shows the Icorr values during the monitored period for the samples with 10 cm long reservoir. The remaining sample with a 17.5 solution reservoir, shows recent Icorr values close to 15 μA. Samples embedded in samples with reservoirs of 2.5 to 5 cm long, had rebar Icorr values that ranged between 5 and 10 μA. Four out of five rebars show a modest increase in Icorr measured. Figure 3 shows the Icorr vs. time for the rebars embedded in samples with 5 cm long reservoirs, note that SL-7 and SL-8 were placed in the environmental chamber and hence there are several measurement performed as the sample regained moisture. The images for the other samples can be found in the appendix.

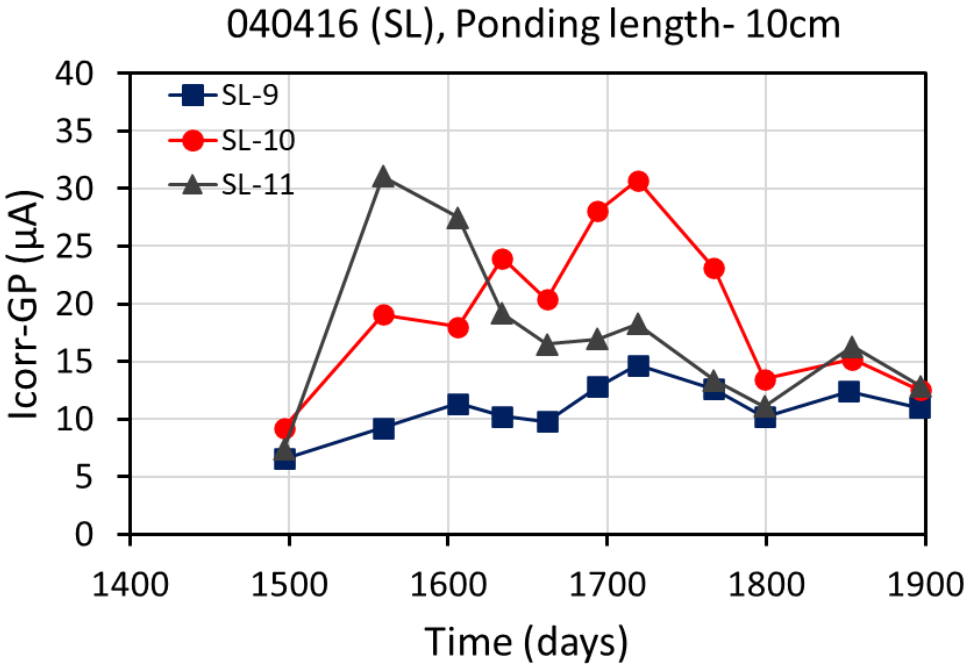

Figure 2. Icorr vs. time for SL single rebar with 10 cm long reservoir

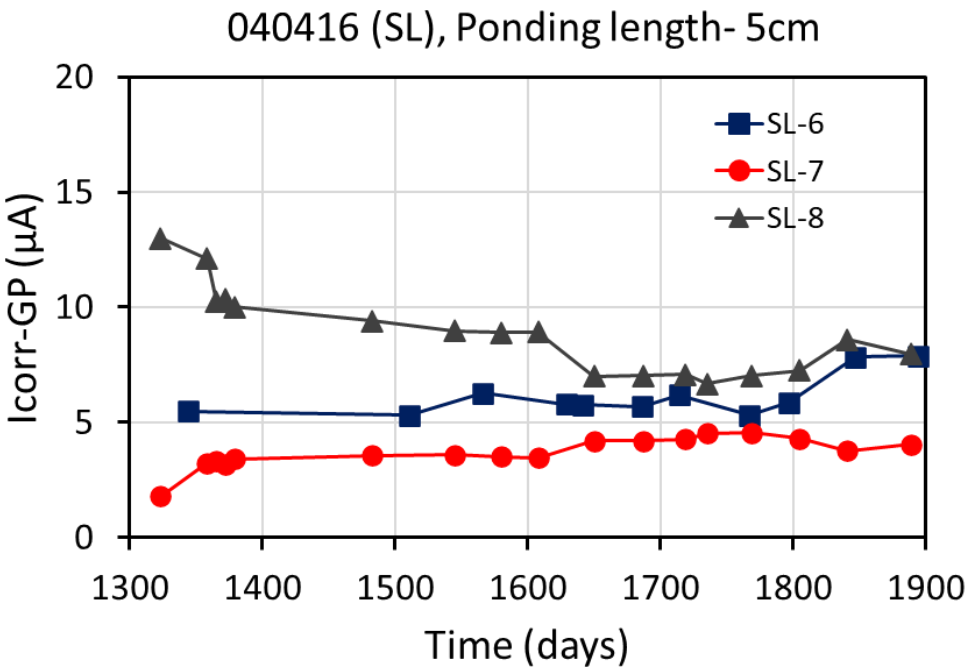

Figure 3. Icorr vs. time for SL single rebar with 5 cm long reservoir

FA single rebar samples.

Two rebars consistently (FA-10 and FA-2, see Figure 4 below) had rebar ICP potential values more negative than -0.4 Vsce, these two rebars also showed higher corrosion currents when compared to the other samples with the same solution reservoir length. The rebars in sample FA2 (5cm) and FA5 (7.5 cm) showed Icorr values > 15 µA several times, but also showed some oscillation (transients) in the measured corrosion current values. Figure 5 show the Icorr and Ecorr values measured on the rebars embedded in FA samples with 5 cm solution reservoir. The other plots can be found in Appendix B.

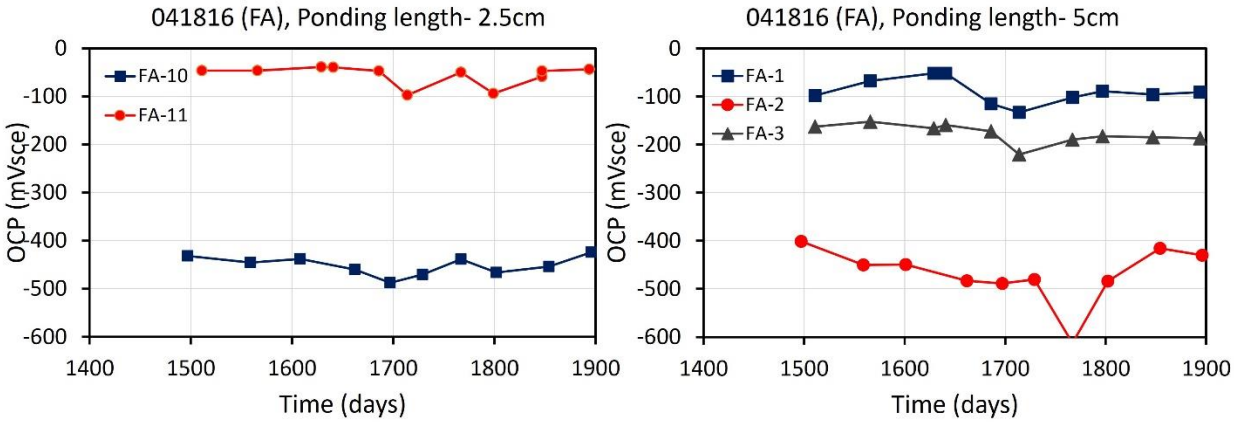

Figure 4. OCP vs. time for selected FA single rebar specimens

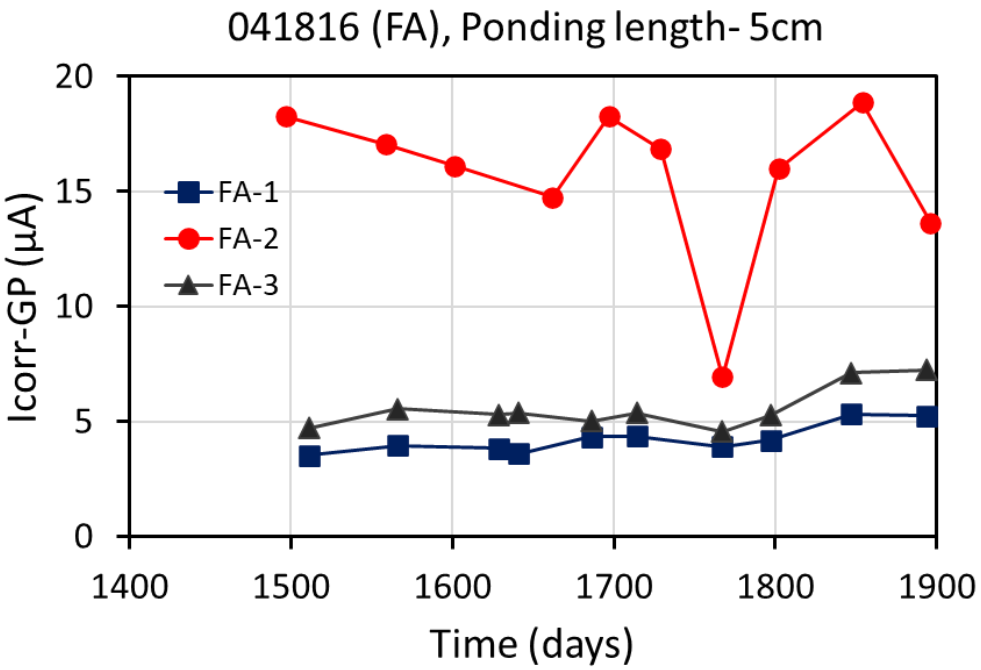

Figure 5. Icorr vs. time for FA single rebars samples with reservoir 5 cm long

Single Rebar T1 samples. The larger Icorr was observed on T1-8 specimens which has a 15 cm long reservoir. During the monitored period reported in here, it started at values ranging between 15 and 20 µA, but the latest Icorr was close to 10 µA (See Figure 6). The other three T1 samples had smaller Icorr values (See appendix B). Samples with reservoir length of 5 cm had Icorr values that changed little over the reported period (~5 µA), the Icorr on the samples with a reservoir of 10 cm tended toward smaller values, and currently is also about 5 µA.

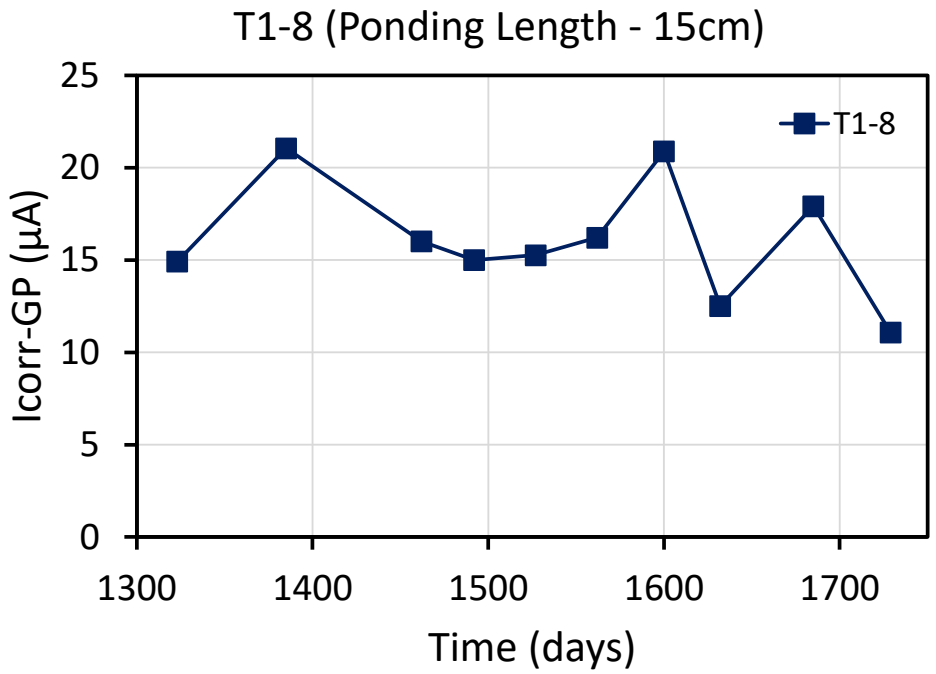

Figure 6. Icorr vs. time for T1-8 single rebar specimen (15 cm long reservoir)

Single Rebar T2 samples. Modest fluctuation in Icorr overtime were observed on the rebars embedded in single rebar T2 samples. The rebar with the most negative potential (T2-1, see appendix B) had the larger Icorr (T2-1, for samples with 5 cm solution reservoir), see Figure 7. Similar Icorr values (around 10 μA) were observed on the rebar embedded in T2-11 specimen (in this case the reservoir is 15 cm long).

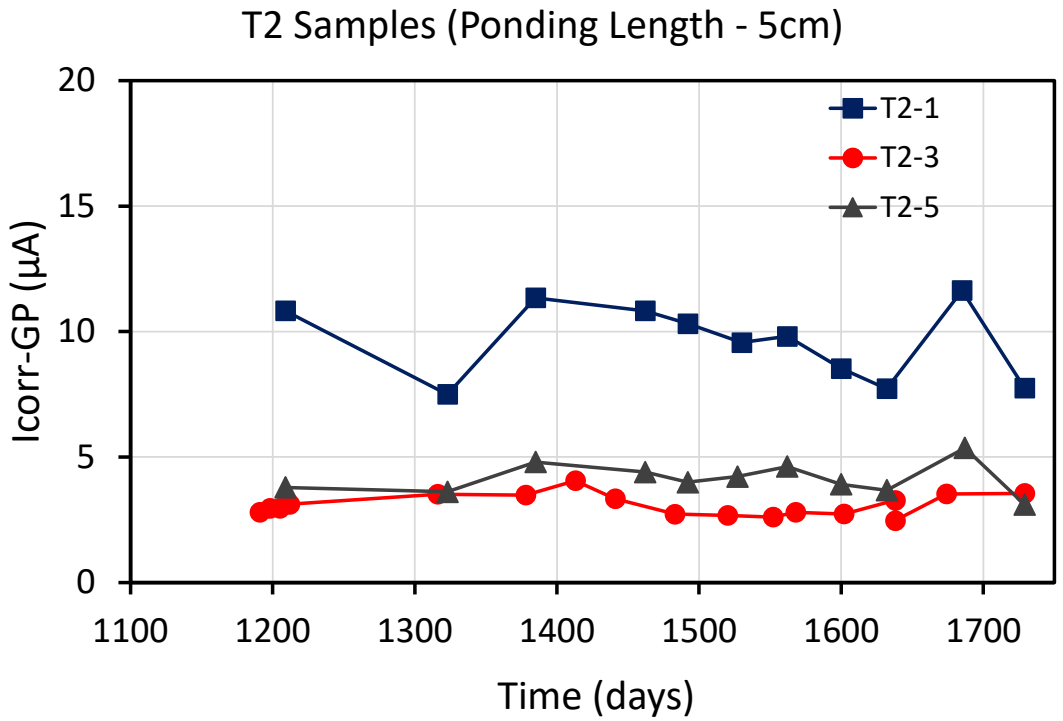

Figure 7. Icorr vs. time for T2 single rebar specimens (5 cm long reservoir)

Three rebar specimens. This section describes how Icorr changed during the monitored period on FA three rebar specimens. Appendix C presents the Icorr observed values on SL, T1 and T2 three rebar specimens. Figure 8 shows how Icorr evolved on rebars of FA specimens with 2.5 cm long reservoir. Most Icorr values measured on three rebar FA specimens with reservoir of 2.5 cm, were less than 8 μA, however sample 11X had values that ranged between 20 and 30 μA, with the last readings being around 10 μA.

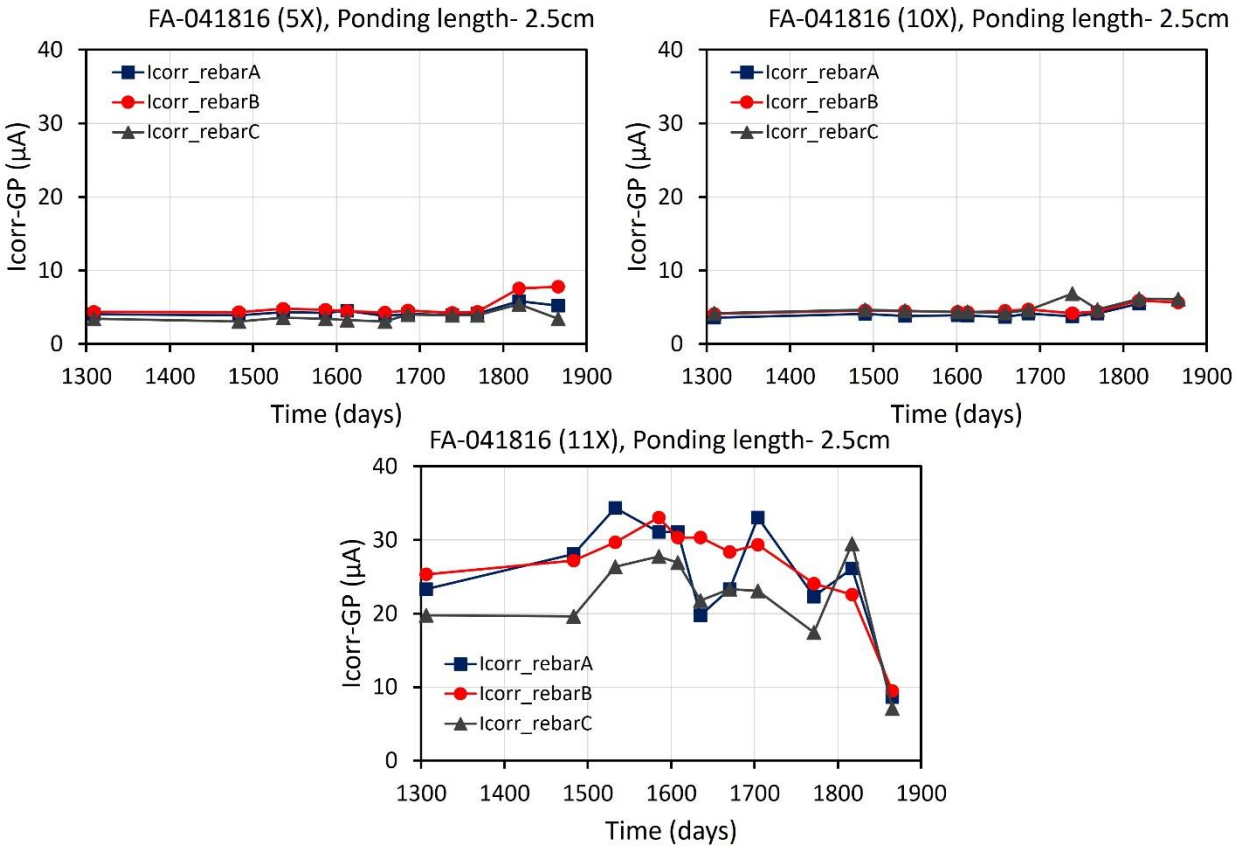

Figure 8. Icorr vs. time for rebars embedded in three rebar FA specimens with 2.5 cm reservoir

Figure 9 shows how Icorr evolved on rebars of FA specimens with 5 cm long reservoir. Over monitored period reported in here, the Icorr remained at constant values on the specimen with lower Icorr values (i.e., 7X), Icorr ranged between 10 and 15 µA (with some fluctuation) on the rebars of sample 23X and the Icorr values were initially constant on the rebars of samples 12X, Rebar C had values as high as 30 µA, more recently the Icorr of this rebar transitioned downwards reaching values of around 12 µA. The trend towards lower Icorr values was also observed on rebars A and B in specimen 12X.

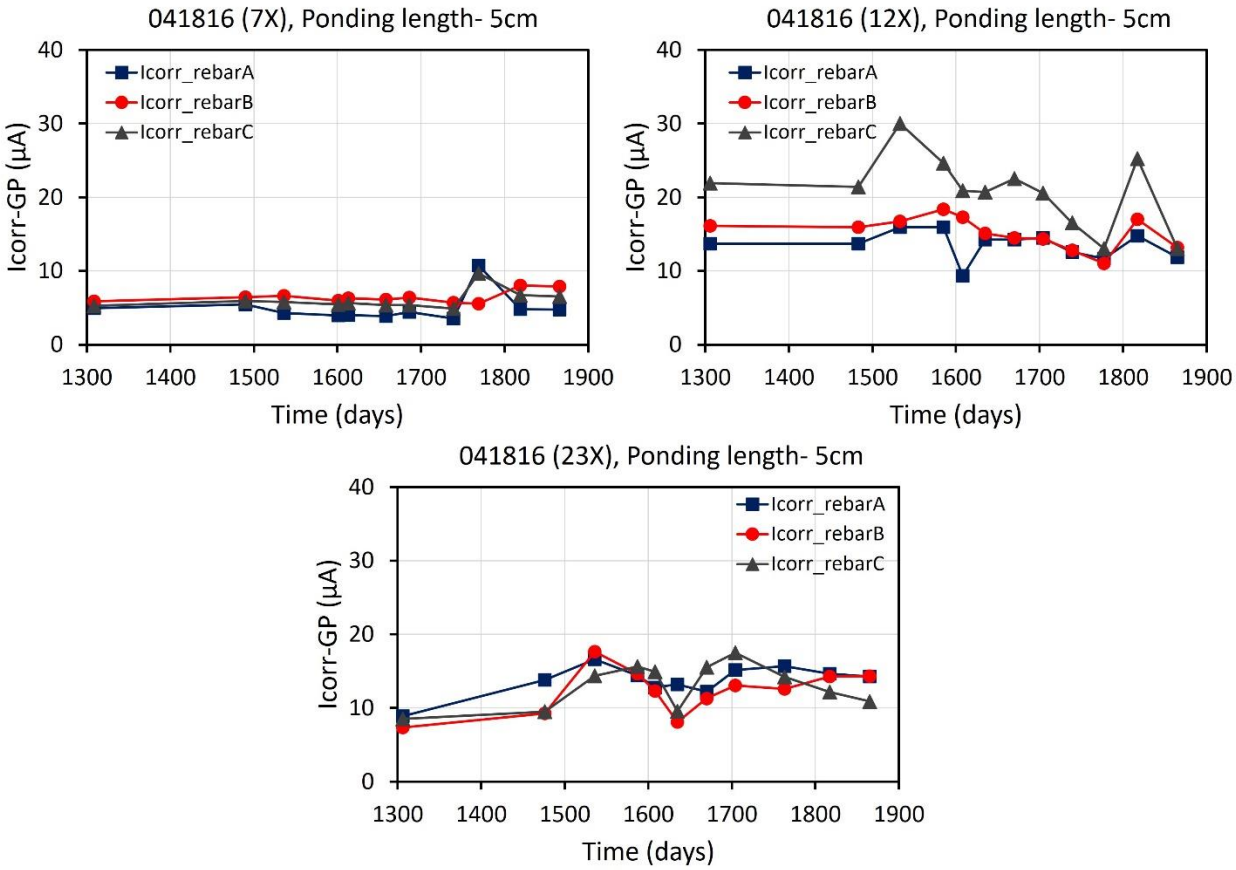

Figure 9. Icorr vs. time for rebars embedded in three rebar FA specimens with 5 cm reservoir

Figure 10 shows the Icorr vs. time for rebars embedded in FA specimens with 10 cm long reservoir. A downward trend in Icorr was observed on the three specimens. The most recent Icorr values ranged between five and 10 µA. Figure 11 shows the Icorr vs. time for rebars embedded in FA specimens with 15 cm long reservoir. On these samples, there was an initial trend down on the Icorr observed followed by an upward trend, but more recent measurement suggest plateau or modest decrease in Icorr values on most rebars. Two exceptions rebar 14X-A and 18X-C. On sample 14X, Icorr reached values as high as 30 µA, but recently it shifter towards Icorr= 10 µA (with one exception). The Icorr values in the other two samples ranged between 10 and 20 µA (with a few values slightly larger than that).

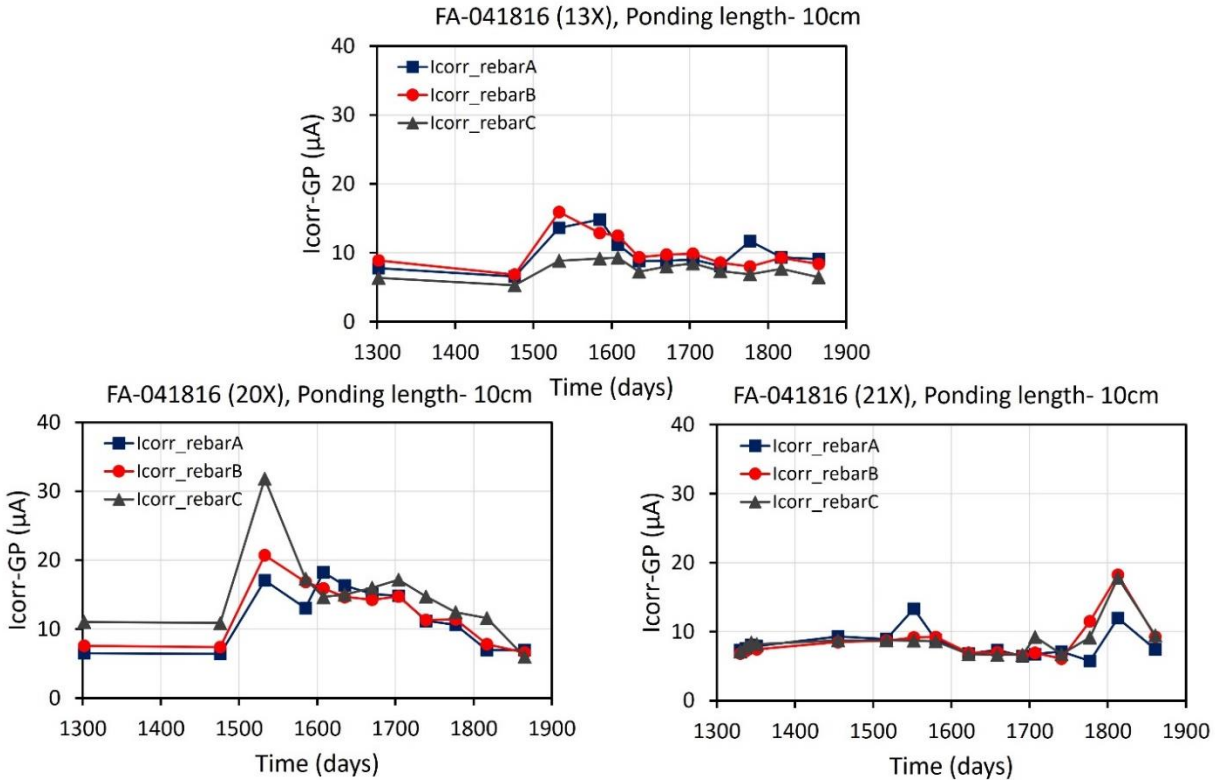

Figure 10. Icorr vs. time for rebars embedded in three rebar FA specimens with 10 cm reservoir

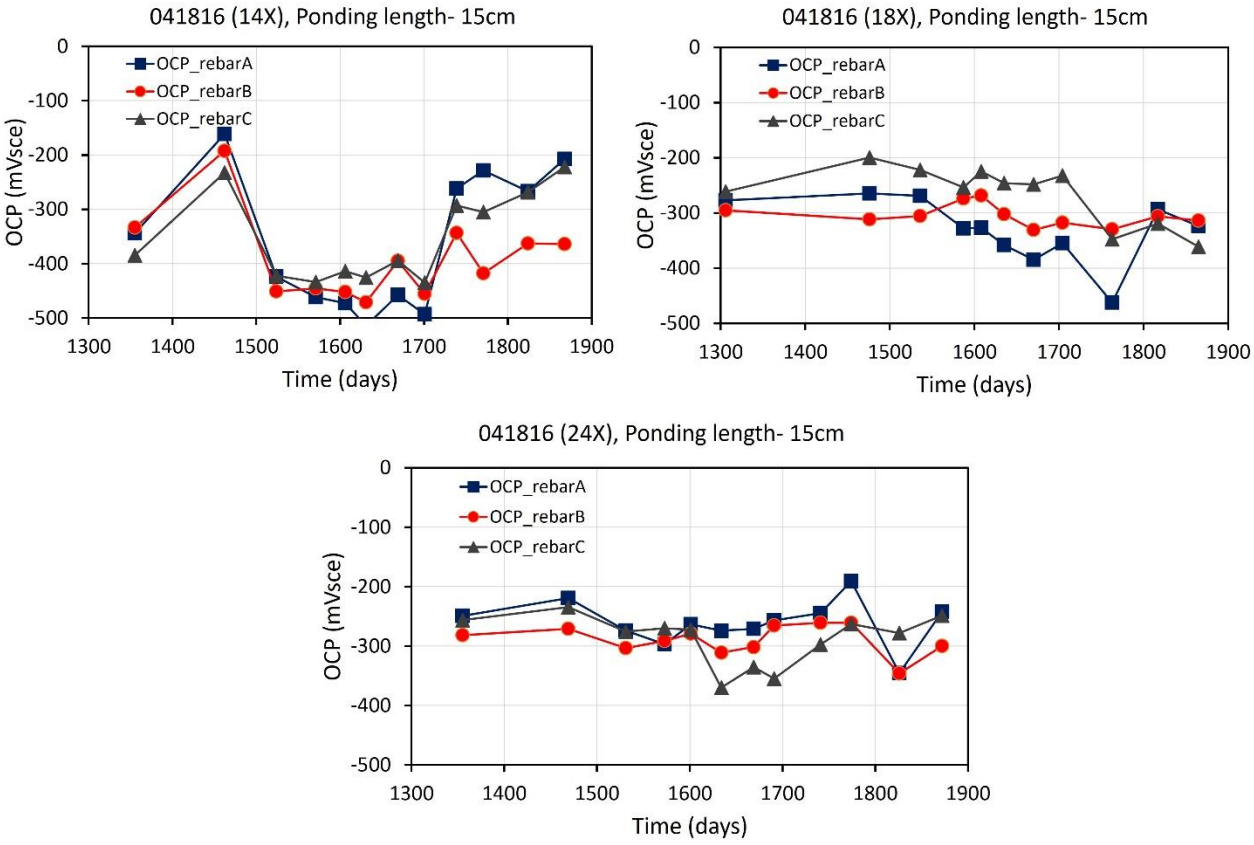

Figure 11. Icorr vs. time for rebars embedded in three rebar FA specimens with 15 cm reservoir

Outdoor Specimens

This section describes plots of Icorr vs. time and Ecorr vs. time for selected samples for a variety of compositions. The outdoor samples had been exposed for close to 26 years, day zero in the plots is with respect to when the samples started to be monitored as part of the TriDurLE project. Figure 12 shows on the left plots of how Icorr changed with time and on the right the plots show how the rebar potential changed with time. The two samples correspond to the mix with only OPC, with a concrete cover of XX cm. Based on the magnitude of the current Rebar AO5-B shows the larger Icorr from those displayed in here.

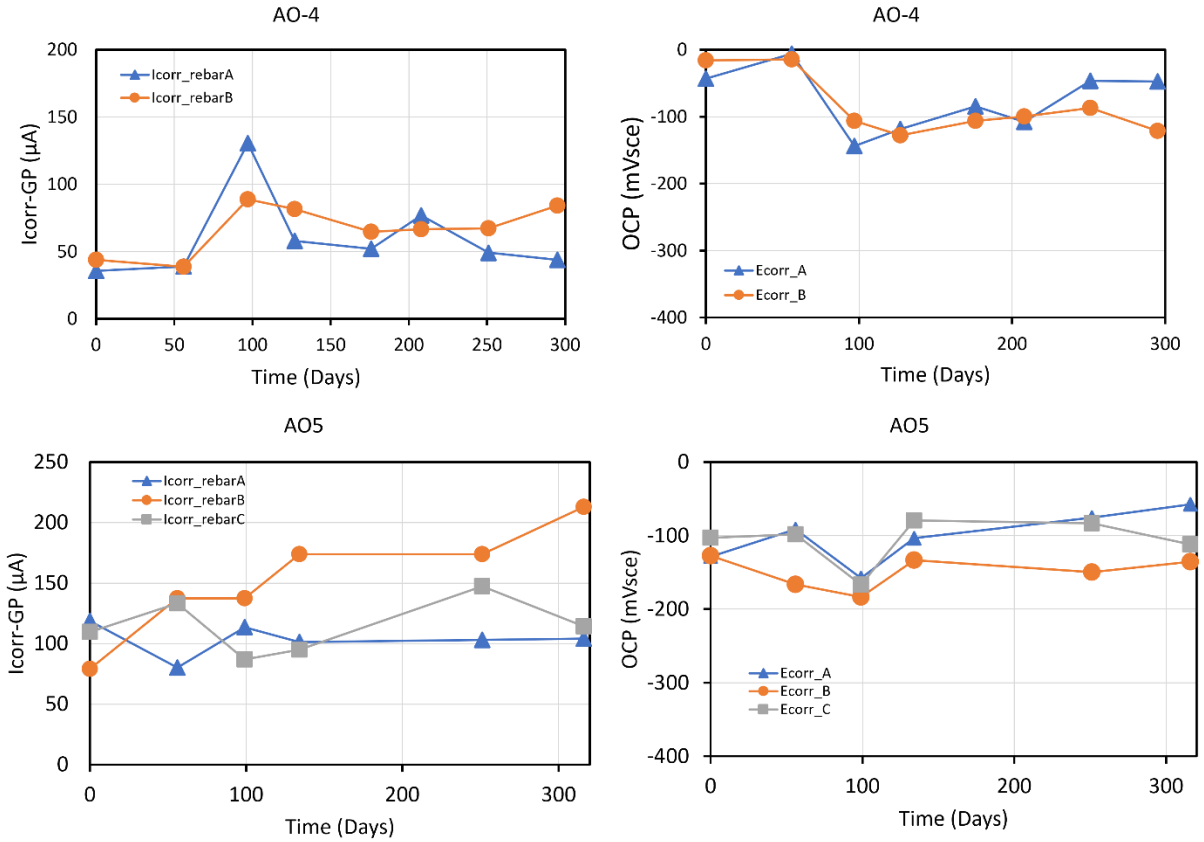

Figure 12. Icorr vs. time and OCP vs time for two AO samples.

Figure 13 shows similar plots for samples with Calcium nitrate added to the base mix. All rebars show a corrosion current greater than 200 µA for most of the monitored period. The rebar potential for all rebars is currently more negative than -300 mVsce, suggesting that all rebars are in the corrosion propagation stage. (Add which from these samples there are cracks on top of which rebars).

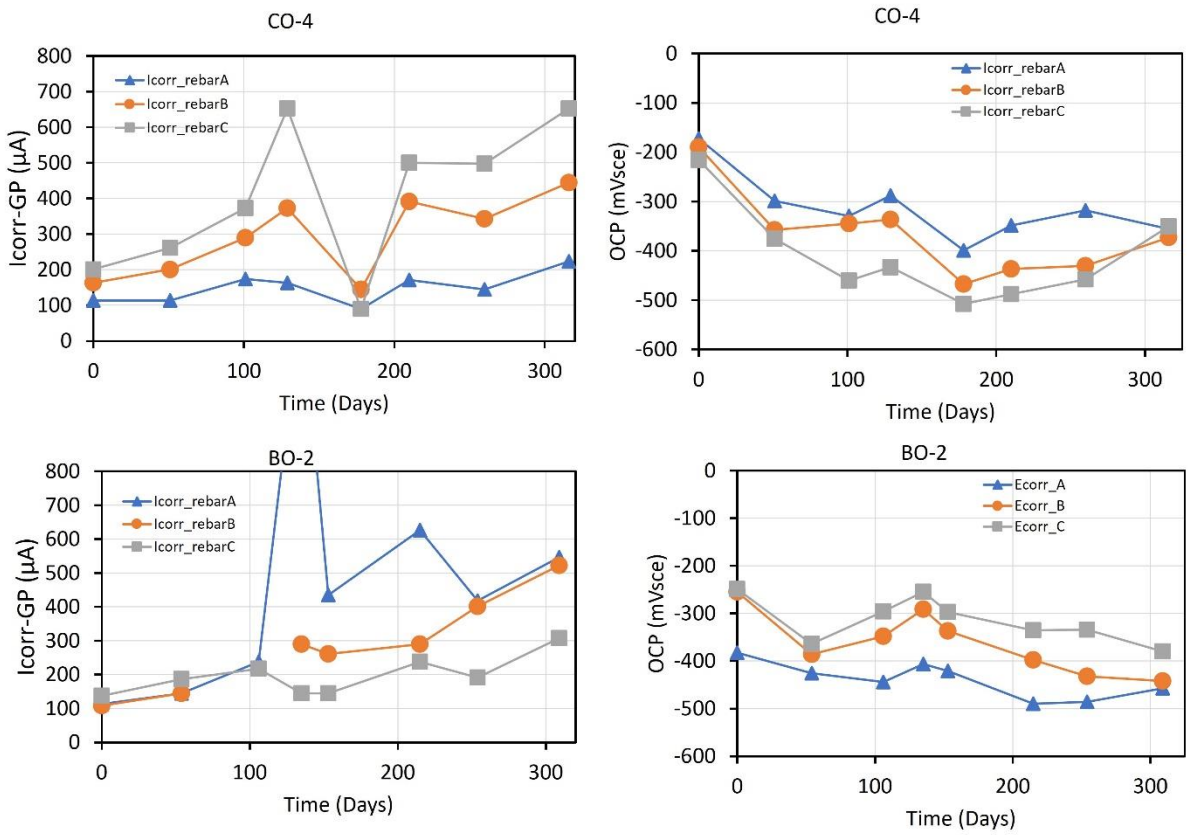

Figure 13. Icorr vs. time and OCP vs time for two CO/BO samples.

Figure 14 shows plots for two samples with fly ash (intermediate amount of FA). Two rebars in sample FA2-7 and one rebar (C) in sample FA2-3 showed Icorr greater than 100 µA for all or part of the monitoring period. The rebar potential on rebar FA2-3-C showed a transition from positive to negative and back to positive rebar potential values, whereas the two rebars with negative ocp values in FA2-7 showed values of -200 mVsce or more negative, with both rebars being around -300 mVsce at the end of the monitored period. Typical values observed on rebars embedded in SF3 and SF4 composition are shown in Figure 15 and Figure 16, respectively. On average the rebars in sample SF3-1 showed corrosion currents that were almost double those observed on rebars in SF3-3 sample. The rebar potentials were more positive than those observed on FA, CO or AO samples described above. The rebars embedded in SF4 concrete showed rebar potential values nobler (more positive than) -100 mVsce, except for the last measurement on two rebars embedded in SF4-1 samples. Most rebar values observed were around 50 µA, with a few cases in which rebars in SF4-1 exceeded 100 µA, suggesting that two of the rebars in SF4-1 are more active than the rebars embedded in SF4-2 sample.

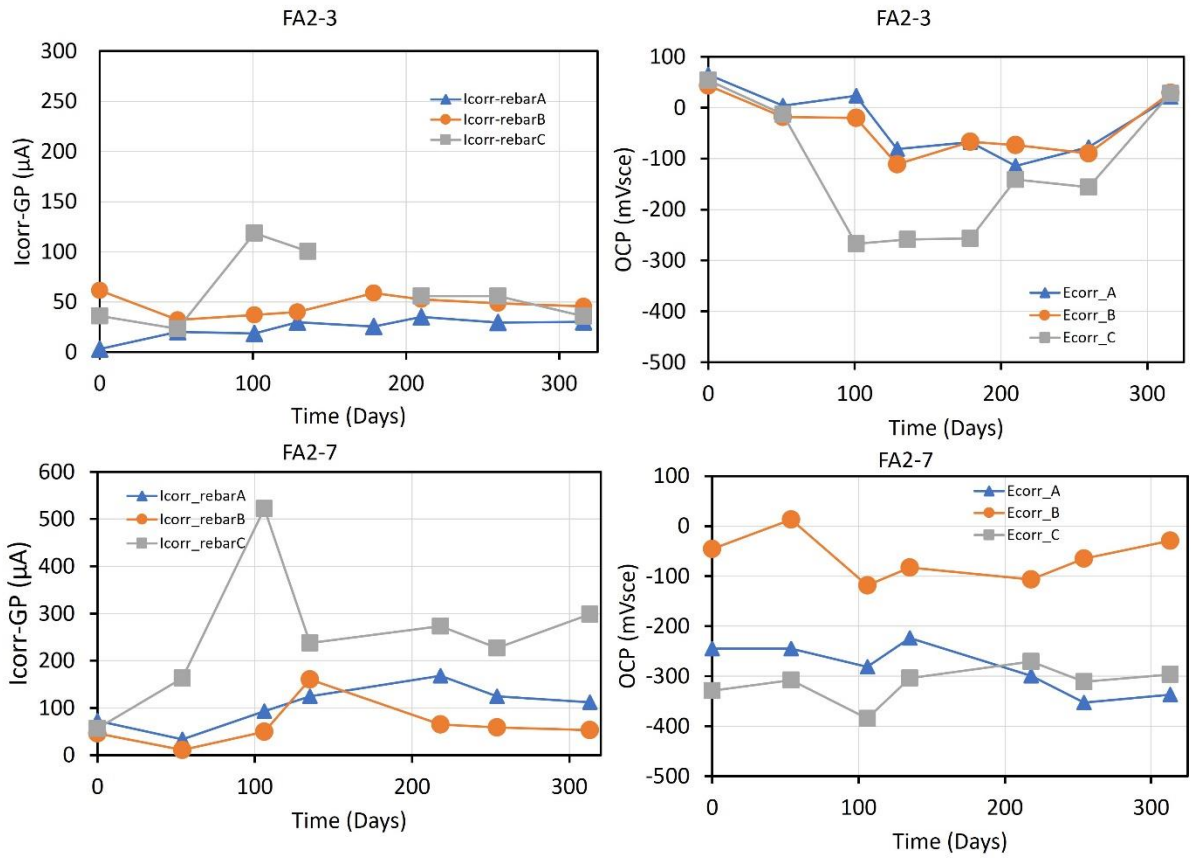

Figure 14. Icorr vs. time and OCP vs time for two FA2 samples.

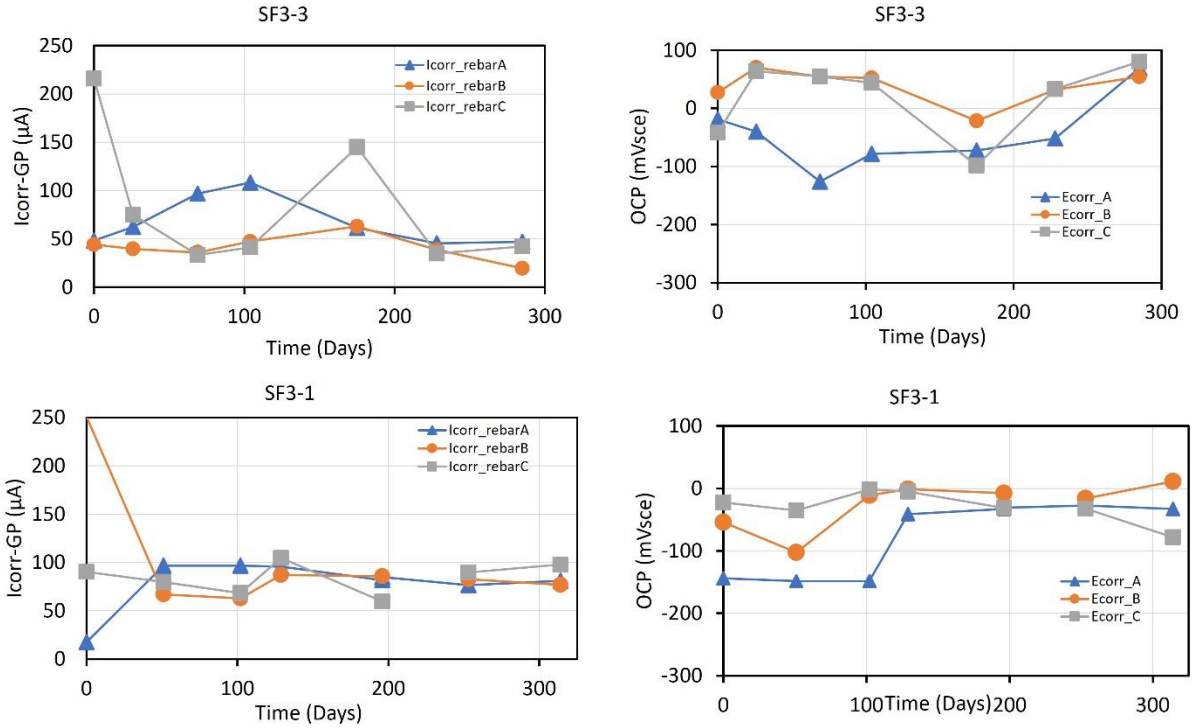

Figure 15. Icorr vs. time and OCP vs time for two SF3 samples.

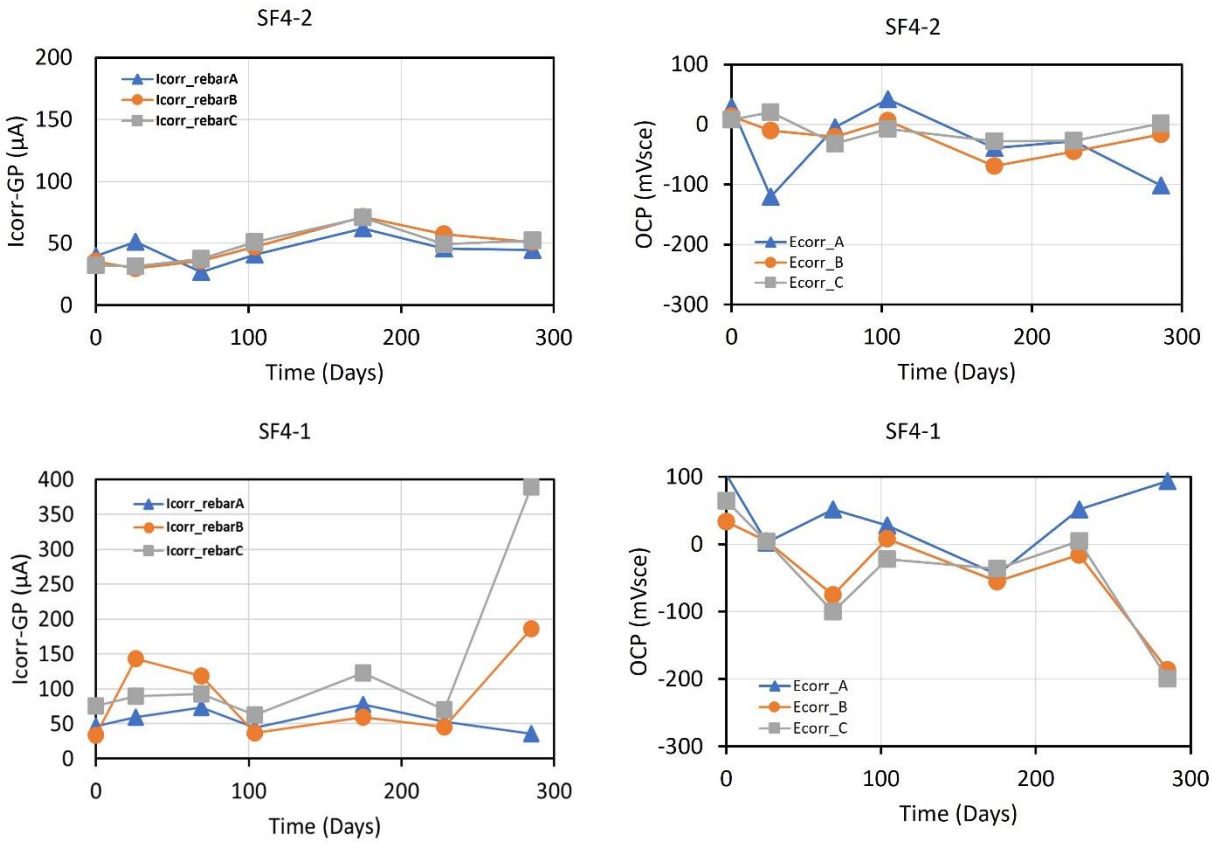

Figure 16. Icorr vs. time and OCP vs time for two SF4 samples.

Correlations: Indoor Specimens

Rs vs. Icorr. Correlations plots were prepared using three values (and averaged per each rebar) measured between May and August 2021. This gives a sense of the recent state of the progression correlating the solution resistance and Icorr measured values. The correlations observed on the single rebar specimens are shown in Figure 17. The slopes observed on rebars of samples in SL and FA concrete are somewhat different from the slope observed on rebars in T1 and T2 samples, the slope for the latter were stepper. A greater scatter was observed on values measured on FA single rebar specimens. For example, the FA plot shows that in one instance the Icorr was larger for a rebar with 5 cm reservoir length compared to rebars with 7.5 cm long reservoir (FA) and that the Rs was comparable (or slightly larger Rs on the 5 cm long reservoir sample). The correlation observed on values from T1 and T2 rebars also showed overlap, but this was not observed on SL single rebar samples.

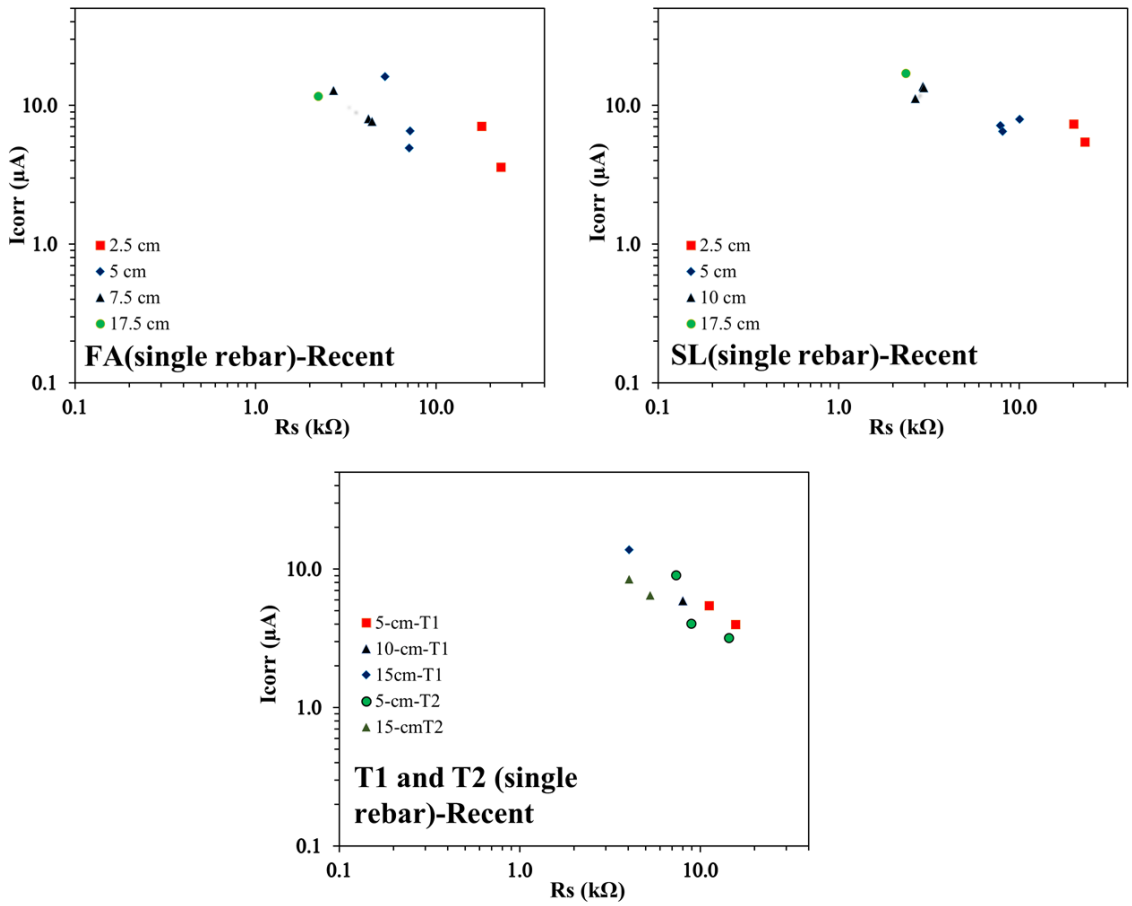

Figure 17. Single rebar Rs vs. Icorr correlation

The Rs vs. Icorr correlations corresponding to three rebar specimens are shown in Figure 18. In general, the Rs values on the three rebar specimens tended to be smaller than those observed on the single rebar specimens (when comparing rebars embedded in the same type of concrete). The rebars embedded in SL concrete showed the most scatter, followed by rebars embedded in FA specimens. Rebars embedded in FA concrete with the longest reservoir showed the lower Rs and larger Icorr (but there is some spread in the values, particularly along the Icorr values. Correlations from rebars embedded in T1 and T2 concrete showed less scatter. The T1 and T2 plots showed somewhat larger Rs values with corresponding somewhat lower Icorr values. The ternary nature on T1 and T2 concrete might in part explain the larger Rs values.

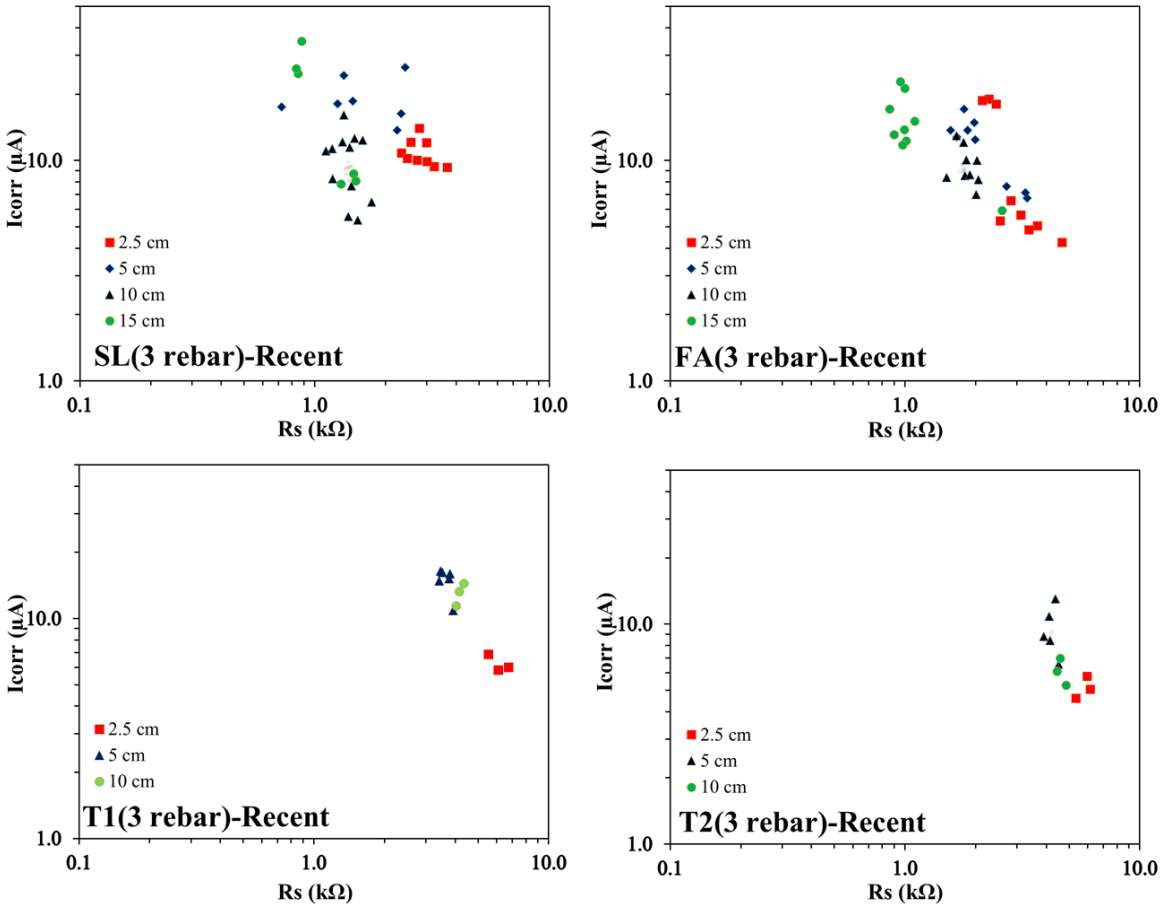

Figure 18. Three rebar specimens: Rs vs. Icorr correlation

Icorr vs. Ecorr. Similar correlations were prepared using the Icorr values vs. Ecorr (OCP) values for each rebar. The plots display the average values per rebar using three measurements (May to August 2021). The series in the plots are also grouped per solution reservoir length and the plots indicate the concrete composition for a given sample set. Plots were prepared for single rebars and another plot for three rebar specimens (Indoor specimens). Figure 19 shows the Icorr vs. Ecorr correlations obtained using the values for the single rebar specimens. Expected trends were observed, but there were a few outliers for two FA values. Two data points showed lower potentials, which might suggest partial mass transport limitation, or that these samples are in a transitional state.

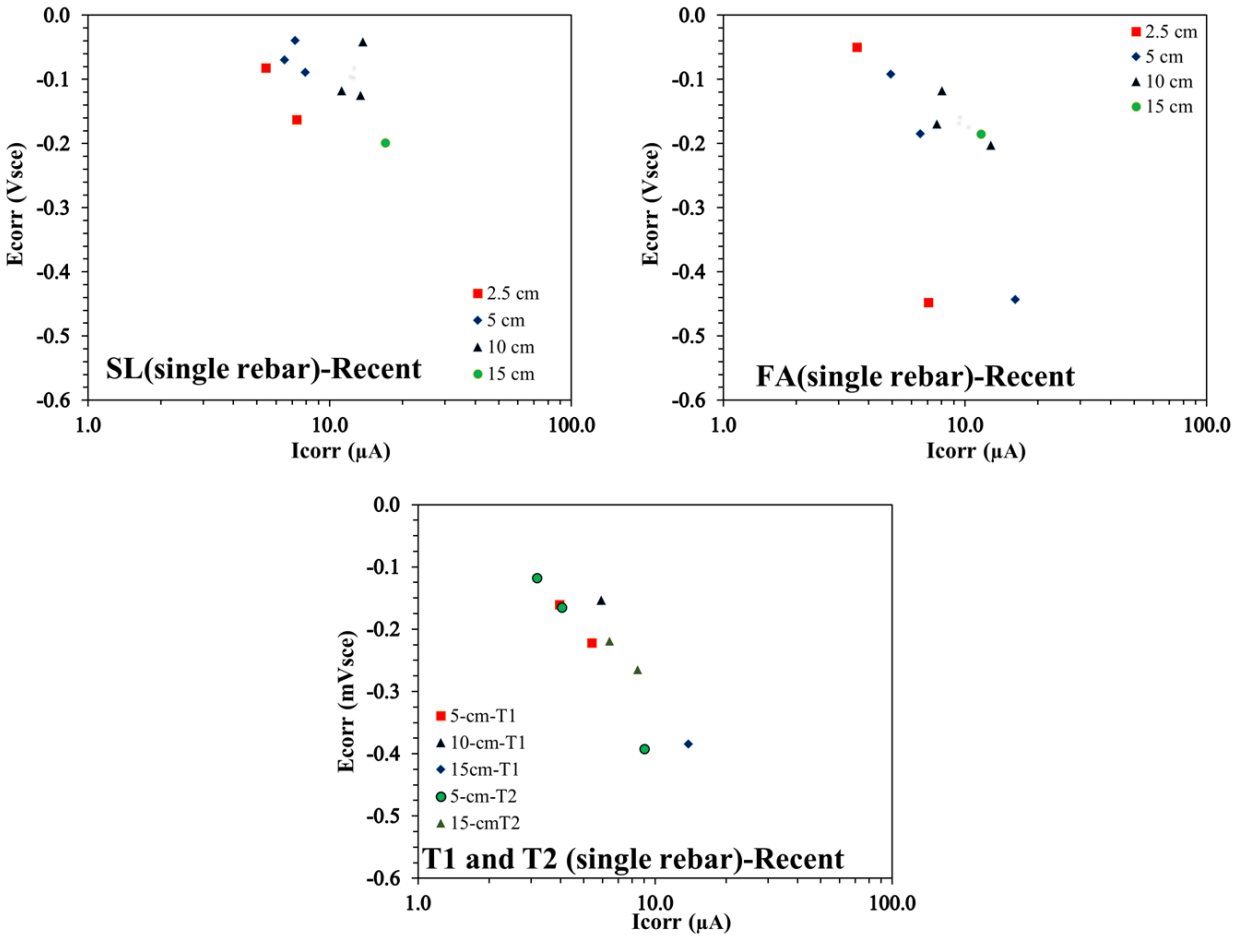

Figure 19. Icorr vs. Ecorr (single rebar specimens)

The Icorr vs. Ecorr correlations from three rebar specimens are shown in Figure 20. A very good correlation was obtained using SL samples, whereas for FA, T1 and T2 the correlations were good, with a few outliers. For FA, T1 and T2, the samples with 2.5 cm long reservoir had the smaller Icorr values, but this was not observed on SL specimens.

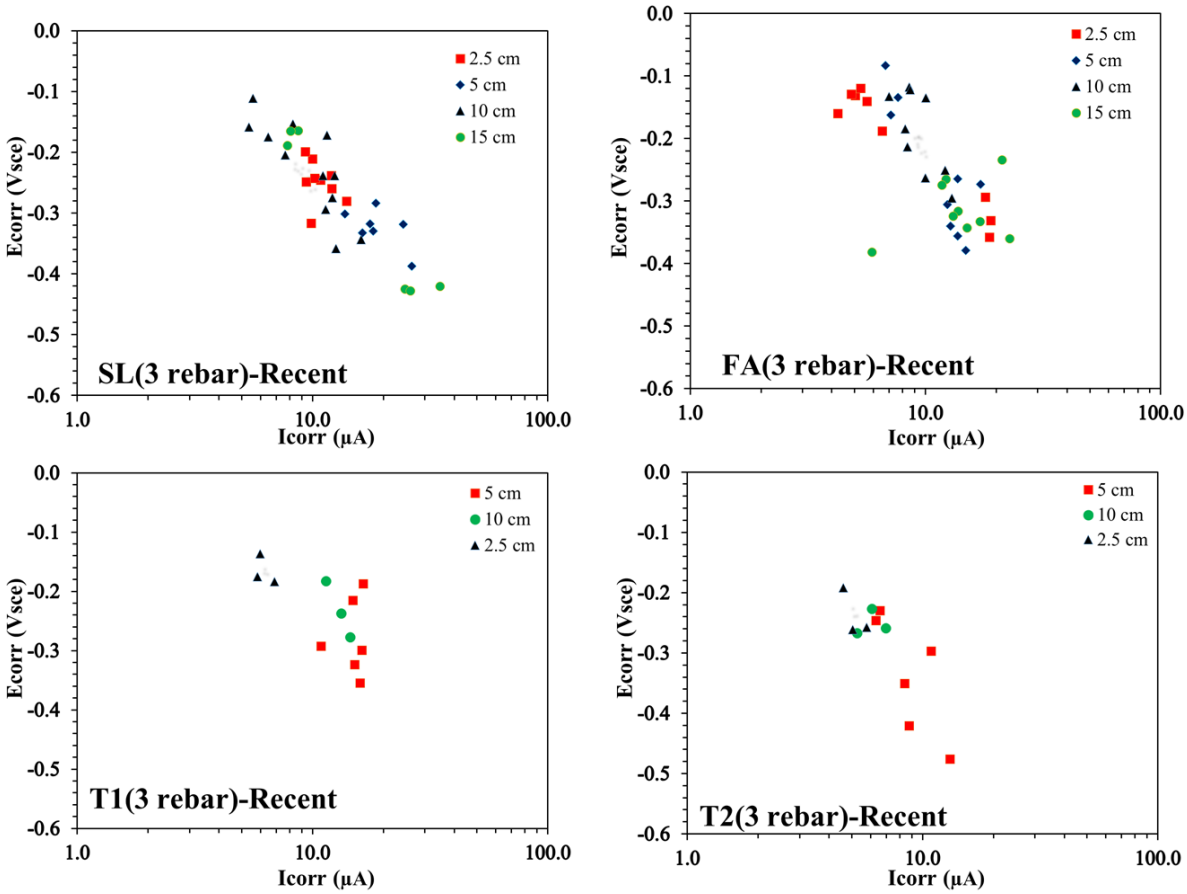

Figure 20. Icorr vs. Ecorr for three rebar specimens (recent readings)

The Icorr vs. Ecorr correlation that had the best trend (less scatter) corresponded to rebars from the SL group.

Correlations: Outoor Specimens

Figure 21 shows the correlation between Rs and Icorr for the outdoor samples. The samples with the smaller Rs tended to have the larger corrosion current. The Rs ranged between 0.1 and 8 Kohm. Most embedded rebars with Rs values smaller than 0.5 Kohms showed cracks. At least 15 rebars exceeded an average corrosion current of 200 µA (using the measured values obtained between April and August 2021), these rebars showed Rs values smaller than 0.8 Kohms. Samples identified with an asterisk symbol correspond to rebars embedded in samples with unknown composition (U-comp)

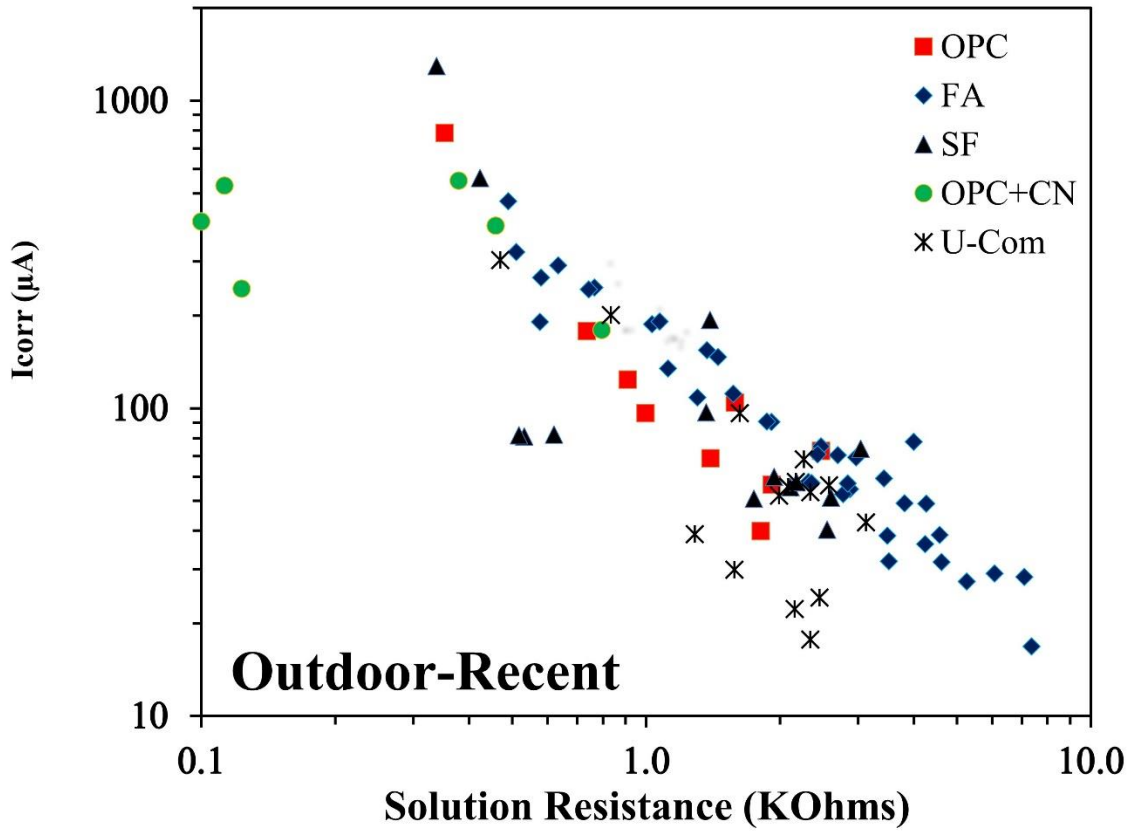

Figure 21. Outdoor samples correlation between Icorr and solution resistance

The correlation between Icorr vs. Ecorr appear to suggest that most samples are undergoing corrosion, but not all at the same rate (See Figure 22). Some rebars with potential values as negative as -250 mVsce have smaller corrosion current (~ <= 40 µA) than rebars with similar rebar potential values (between 100 and 200 µA), suggesting that a smaller area is active on those with smaller currents. Rebars with Icorr values greater than 100 µA are likely to be in the active state (actually rebars with corrosion currents greater than 50 µA could also be in the active state but either corroding at a lower rate or with smaller corroding site(s)). Due to mix rebar potential control, several rebars with potential ~ -100 mVsce showed corrosion currents >100 µA. Rebars with Ecorr < -250 mVsce (i.e., more negative) could be considered to be in a more persistent active state as most rebars with this potential values showed corrosion current in excess of 100 µA (a number of the rebars were found to have average Icorr values ranging between 200 and 1100 µA).

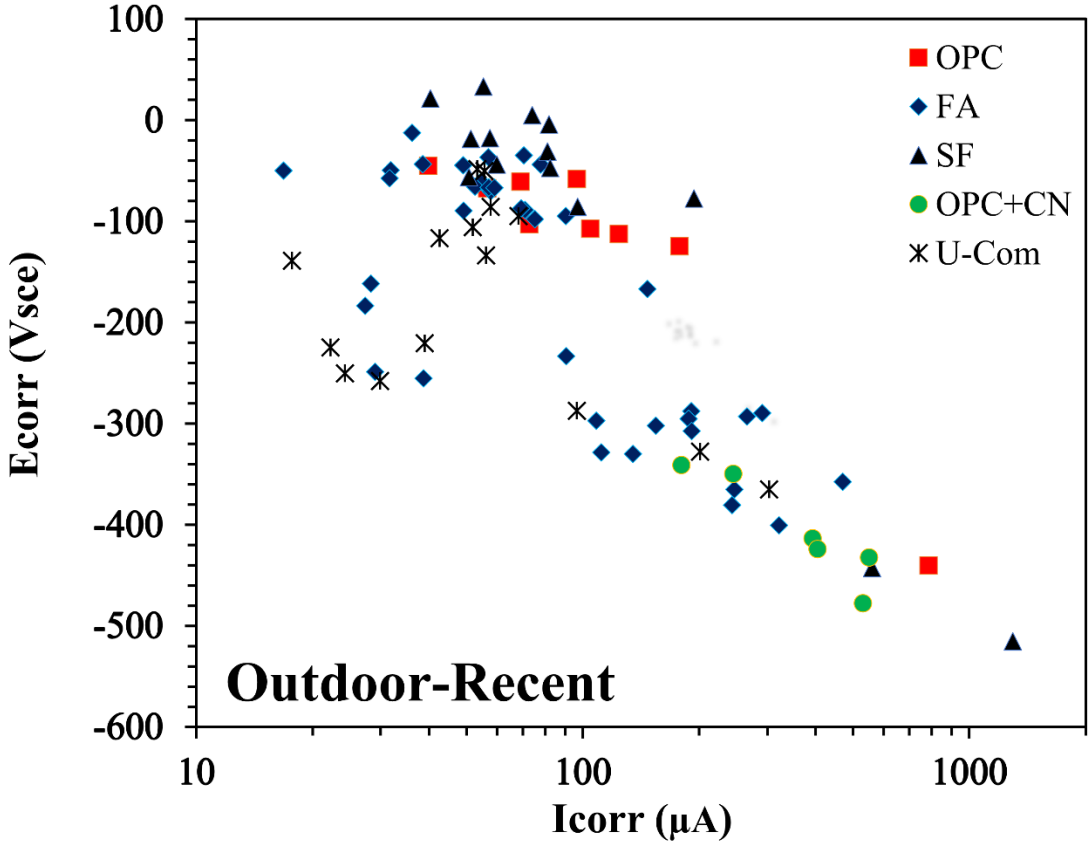

Figure 22. Outdoor samples correlation between Ecorr and Icorr

Mass loss calculations: Indoor Specimens

The tables presented in this section used Icorr values obtained from GP measurements for the period March 2017 to August 2021. (GP was not used during Fall 2016 and Early 2017, LPR measurements were made during that, but are not included in the values reported in here). Table 6 shows the mass loss calculated using Faraday's law and after integrating to obtain the total charge on single rebar specimens. Each row also indicates the sample ID and the length of the solution reservoir in each sample. Rebar SL-3 had the largest mass loss, and corresponded to 0.64 grams, for FA the largest mass loss was calculated for the rebar in FA-4 specimen (0.53 grams), the rebar in T1-9 showed a mass loss of 0.55 grams, and the rebar in T2-2 showed a mass loss of 0.34 grams. No values are shown for the samples that were terminated as part of a previous effort.

Table 6: Mass loss estimated for rebars embedded in single rebar specimens

	grams	Reservoir length (cm)
SL-1		
SL-2		
SL-3	0.64	17.5
SL-4	0.21	2.5
SL-5	0.27	2.5
SL-6	0.26	5
SL-7	0.35	5
SL-8	0.45	5
SL-9	0.39	10
SL-10	0.54	10
SL-11	0.52	10
T1-7	0.25	5
T1-8	0.50	15
T1-9	**0.55**	10
T1-10	0.16	5

	grams	Reservoir length (cm)
FA-1	0.17	5
FA-2	0.42	5
FA-3	0.34	5
FA-4	0.53	7.5
FA-5	0.50	7.5
FA-6	0.49	7.5
FA-7	0.40	17.5
FA-8		
FA-9		
FA-10	0.23	2.5
FA-11	0.12	2.5
T2-1	0.29	5
T2-2	**0.34**	15
T2-3	0.17	5
T2-5	0.14	5
T2-11	0.26	15

Table 7 shows the calculated mass loss obtained from the three rebar specimens. Table X shows three values per row, each in grams corresponding to rebar A, B and C. The two columns on the left indicate the concrete type and reservoir length, and the second column the sample ID. Currently the rebars with the largest mass loss per mix correspond to 4X-C (SL, 15 cm) 1.34 grams, 12X C (FA 5 cm) 0.78 grams, 27X C (T1 2.5 cm) 0.69 grams and 29X-A (T2 10 cm) 0.44 grams. The table show that in some cases the three rebars in a given sample had very similar mass loss, as for example sample 3X, but in other cases one of the rebars had a significantly larger (e.g., 1X-C) or smaller (eg. 2X-C) calculated mass.

Table 7: Estimated mass loss for rebars in three rebar specimens (values in grams)

		A	B	C
SL-5 cm	1X	0.49	0.42	0.64
SL-2.5cm	2X	0.40	0.41	0.34
SL-10cm	3X	0.21	0.22	0.22
SL-15cm	4X	0.59	0.75	**1.34**
FA	5X	0.19	0.20	0.19
SL-10 cm	6X	0.63	0.39	0.45
FA	7X	0.29	0.27	0.25
SL-10cm	8X	0.30	0.26	0.21
SL-2.5cm	9X	0.47	0.59	0.48
FA-2.5cm	10X	0.17	0.20	0.21
FA-2.5cm	11X	0.76	0.80	0.63
FA-5cm	12X	0.66	0.72	0.78
FA	13X	0.40	0.40	0.28
FA-15 cm	14X	0.69	0.40	0.65
SL 10cm	15X	0.43	0.40	0.39
SL	16X			0.76
SL-5cm	17X	0.69	0.64	0.72
FA-15cm	18X	0.45	0.42	0.35
SL-2.5cm	19X	0.61	0.32	0.36
FA-10cm	20X	0.33	0.37	0.46
FA-10 cm	21X	0.47	0.53	0.52
SL-15cm	22X	0.30	0.25	0.27
FA-5cm	23X	0.48	0.41	0.47
FA-15cm	24X	0.48	0.64	0.49
T1-2.5cm	25X	0.54	0.58	0.69
TX-2.5cm	26X	0.36	0.37	0.32
TX-10cm	27X	0.54	0.57	0.61
T1-5cm	28X	0.26	0.29	0.27
T2-10cm	29X	0.44	0.29	0.27
T2-2.5cm	30X	0.22	0.19	0.19
T2-5cm	31X	0.26	0.36	0.20
T2-5cm	32X	0.31	0.31	0.37

Chapter 5. Summary and Conclusions

The results and discussion section provides insight on how the corrosion has propagated during the reported period. It also indicates that the calculated mass loss (indoor samples) for most rebars is moderate, but in some cases surpasses the amount that caused cracks on Busba [20] and Torres [10] study. It is possible that the corrosion is taking place in a more localized manner and also under higher moisture (which could be allowing corrosion products to mover farther within the concrete pore-structure). Longer periods with no solution might provide time for ferrous/ferric hydroxides to be transformed to oxidized state.

References

1. U. Angst, B. Elsener, A. Jamali, and Adley, “Concrete cover cracking owing to reinforcement corrosion-theoretical considerations and practical experience”, Materials and Corrosion, Volume 63, No 12, page 1069-1077, 2012
2. M.D.A. Thomas and J.D. Matthews, “Chloride penetration and reinforcement corrosion in marine-exposed fly ash concretes”. In: Malhotra VM, editor, Third CANMET/ACI International Conference on Concrete in a Marine Environment, ACI SP-164, Detroit: American Concrete Institute; p. 317-38 1996
3. F. Presuel-Moreno, M. Paredes, “16 Years’ Exposure Of Fly Ash And Silica Fume Concretes On Salt Induced Reinforcing Steel Corrosion: Corrosion Potential, Resistivity And Diffusivity”, International Conference in Durability of Concrete, Trondheim, Norway, June 18-21, 2012 (Proceeding published on USB/Electronic form)
4. C Andrade, C Alonso “Test methods for on-site corrosion rate measurement of steel reinforcement in concrete by means of the polarization resistance method” Materials and Structures, v37 p623, 2004
5. W. Morris, A. Vico, M. Vázquez, “Chloride induced corrosion of reinforcing steel evaluated by concrete resistivity measurements” Electrochemica Acta, V 49 pp4447–4453 2004
6. F.J. Presuel, R. Bencosme, K. Hoque, M.Nazim, F. Tang, A. Kazemi, “Corrosion Propagation of Carbon Steel Rebars in High Performance Concrete”, BDV27–977–08, Florida Atlantic University, Final report for FDTO, November 2018
7. Tutti, K. 1982. “Corrosion of Steel in Concrete.” Swedish Cement and Concrete Research Institute, 4-82.
8. Otieno, M., Beushausen, H., & Alexander, M. (2012). Prediction of corrosion rate in reinforced concrete structures–a critical review and preliminary results. Materials and Corrosion, 63(9), 777-790.
9. Liu, Y., and Weyers R. 1998. “Modeling the Time to corrosion Cracking in Chloride Contaminated Reinforced Concrete Structures.” ACI Materials Journal, Vol. 95, No. 6, pp. 675-681.
10. Torres-Acosta, Andres A., and Alberto A. Sagues. 2004. “Concrete Cracking by Localized Steel Corrosion-Geometric Effects.” ACI Materials Journal 101 (6): 501-7
11. Marcotte, T.D. 2001. “Characterization of Chloride-Induced Corrosion Products that Form in Steel-Reinforced Cementitious Materials.” Ph.D. Thesis in Mechanical Engineering, University of Waterloo: Waterloo, Canada
12. Hansson, C., Poursaee, A. and Jaffer, S. 2007. “Corrosion of Reinforcing Bars in Concrete.” Portland Cement Association, PCA R&D Serial No. 3013, Skokie, Illinois
13. Bentur, A., S. Diamond, N. Berke. 1997. “Steel corrosion in concrete.” Fundamentals and Civil Engineering Practice., 41-43, E & FN Spon, London
14. Scott, A.N., M.G. Alexander. 2007. “The influence of binder type, cracking and cover on corrosion rates of steel in chloride-contaminated concrete.” Mag. Concr. Res. 59 (7), 495–505
15. Otieno, M., H. Beushausen, and M. Alexander. 2010 “Corrosion in cracked and uncracked concrete-influence of crack width, concrete quality and crack re-opening.” Mag. Concr. Res. 62 (6) 393-404.
16. Melchers, R. E., and I. A. Chaves. 2019. “Durability of reinforced concrete bridges in marine environments.” Structure and Infrastructure Engineering, DOI: 10.1080/15732479.2019. 1604769, ISSN: 1573-2479.
17. Jamali, Amin, Ueli Angst, Bryan Adey, and Bernhard Elsener. 2013. “Modeling of Corrosion-Induced Concrete Cover Cracking: A Critical Analysis.” Construction and Building Materials 42: 225-37.
18. Otieno, M., M. G. Alexander, and H. Beushausen. 2009. “Corrosion propagation in cracked and

uncracked concrete." University of Cape Town, Cape Town, South Africa, ISBN 978-0-415-46850-3
19. Otieno, M., G. Golden, M. G. Alexander, and H. Beushausen. 2019. "Acceleration of steel corrosion in concrete by cyclic wetting and drying: effect of drying duration and concrete quality." Materials and Structures 52:50.
20. Busba, Ezeddin, and Alberto A. Sagues. 2013. "Critical Localized Corrosion Penetration of Steel Reinforcement for Concrete Cover Cracking." NACE Corrosion 2013 Conference & Expo, no 2747: 1-14
21. Angst, Ueli, B. Elsener, A. Jamali, and Adley. 2012. "Concrete cover cracking owing to reinforcement corrosion-theoretical considerations and practical experience." Materials and Corrosion, Volume 63, No 12, page 1069-1077
22. Angst, Ueli, Bernhard Elsener, Claus K. Larsen, and Oystein Vennesland. 2010, "Considerations on the Effect of Sample Size for the Critical Chloride Content in Concrete." In Proc. 2nd Int. Symp. on Service Life Design for Infrastructures, 569-76. Delft: RILEM Publications S.A.R.L
23. Broomfield, J. (2003). Corrosion of steel in concrete: understanding, investigation and repair. CRC Press
24. Walsh, Michael T, and Alberto A. Sagüés. 2016. "Steel Corrosion in Submerged Concrete Structures-Part 1: Field Observations and Corrosion Distribution Modeling." Corrosion 72 (4): 518-33
25. Sánchez, A. N., and A. A. Sagüés. 2017. "Reinforced Concrete Corrosion Damage Forecast with Potential Dependent Threshold: Sensitivity to System Parameters." Corrosion 2017. New Orleans, Louisiana, USA: NACE International
26. Budiansky, N. D., Hudson, J. L., & Scully, J. R. (2004). Origins of persistent interaction among localized corrosion sites on stainless steel. Journal of the Electrochemical Society, 151(4), B233.
27. Balasubramanian, H. 2019. "Initiation and Propagation of Corrosion in Dry-cast Reinforced Concrete Pipes with Environmental Effects." Ph.D. Dissertation, Department of Ocean & Mechanical Engineering, Florida Atlantic University.
28. Vanama, R. K., & Ramakrishnan, B. (2020). Improved degradation relations for the tensile properties of naturally and artificially corroded steel rebars. Construction and Building Materials, 249, 118706
29. Imperatore, S., Rinaldi, Z., & Drago, C. (2017). Degradation relationships for the mechanical properties of corroded steel rebars. Construction and Building Materials, 148, 219-230.
30. Moreno, E., Cobo, A., Palomo, G., & González, M. N. (2014). Mathematical models to predict the mechanical behavior of reinforcements depending on their degree of corrosion and the diameter of the rebars. Construction and Building Materials, 61, 156-163
31. Rosa-Paga, Angel, 2021 "The impact corrosion has on the degradation of mechanical properties of carbon steel rebars in high performance concrete", MS thesis, Florida Atlantic University

Appendices

Appendix A. Mix Designs of Outdoor Specimens

Table 8. Mix design AO and CO

	AO	CO
Cement, kgs	113.5	113.4
Calcium Nitrite, kgs	0	5.2
Water, kgs	33.3	28.6
Coarse Aggregates, kgs	286.8	286.8
Coarse Aggregates, % excess moisture	2.06	2.5
Fine Aggregates, kgs	215.6	215.6
Fine Aggregates, % excess moisture	1.3	1.5
Unit Weight, kgs/m^3	2,292.5	2,276.4
w/cm ratio	0.37	0.367
RCP Average at 91 Days, C	4896 (High)	6285 (High)
Strength Avg. 28 days (MPa)	44.2	48.1
Cementitious per unit volume, kgs/m^3	399	394.4

Note: 1 kg/m^3 = 1.6842 lb/yd^3 , 1 kg = 2.205 lbs, 1MPa – 145.03 psi

Table 9. Mix design FA1, FA2, FA3, FA4

	FA1	FA2	FA3	FA4
Cement, kgs	90.8	73.8	56.7	73.8
Fly Ash, kgs	22.7	39.7	56.7	39.8
Calcium Nitrite, kgs	0	0	0	5.2
Water, kgs	27.6	27.8	28.0	24.4
Coarse Aggregates, kgs	287.4	287.4	287.4	288.4
Coarse Aggregates, % excess moisture	2.96	2.3	2.3	2.9
Fine Aggregates, kgs	212.4	206.0	199.6	203.8
Fine Aggregates, % excess moisture	2.68	3.68	3.68	3.0
Unit Weight, kgs/m^3	2,263.6	2,247.6	2,231.6	2,231.6
w/cm ratio	0.367	0.37	0.37	0.363
RCP Avg. 91 Days, C	989	713	731	NA
Strength Avg. 91 days (MPa)	53.2	52.9	45.6	44.5
Cementitious per unit volume, kgs/m^3	399	400.4	401	396

Note: 1 kg/m^3 = 1.6842 lb/yd^3 , 1 kg = 2.205 lbs, 1MPa – 145.03 psi, Type F fly ash was used.

Table 10. Mix design SF1, SF2, SF3, SF4

	SF1	SF2	SF3	SF4
Cement, kgs	110.2	104.4	96.6	104.4
Silica Fume, kgs	7.2	19	35.6	19
Calcium Nitrite, kgs	0	0	0	2.68
Water, kgs	25	18.8	10.2	16.6
Coarse Aggregates, kgs	288.4	288.4	288.4	288.4
Coarse Aggregates, % excess moisture	2.65	2.7	2.9	2.9
Fine Aggregates, kgs	217.4	215.2	212.2	215.2
Fine Aggregates, % excess moisture	2.680	2.68	2.68	2.7
Unit Weight, kgs/m^3	2,279.6	2,273.2	2,262.0	*2,265.2*
w/cm Ratio	0.37	0.367	0.368	0.365
RCP Avg. 91 Days, C	2061	720	598	868
Strength Avg. 28 days (MPa)	48.7	50.8	52.6	48.8
Strength Avg. 91 days (MPa)	52.6	52.2	53.0	51.7
Cementitious per unit volume, kgs/m^3	397	397.6	399	396

Note: 1 kg/m^3 = 1.6842 lb/yd^3 , 1 kg, Silica Fume slurry was used and part of the mass counted towards the water

Appendix B. Indoor Single Rebar Specimens: and OCP vs. time

Icorr vs. time

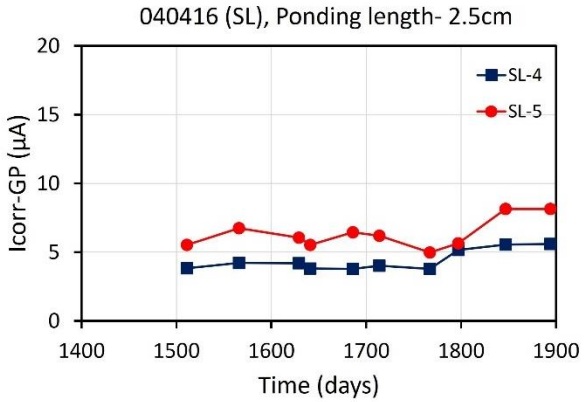

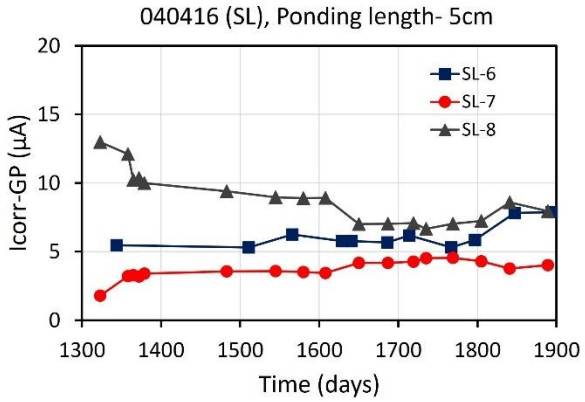

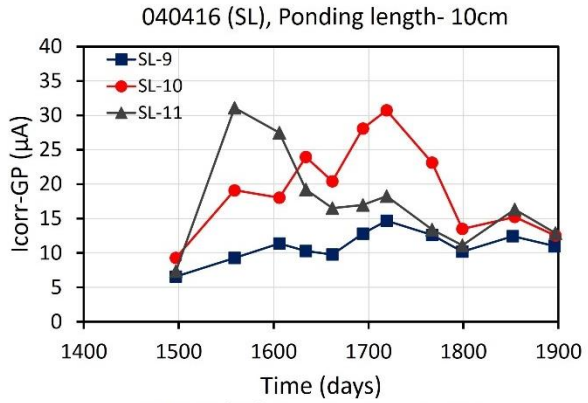

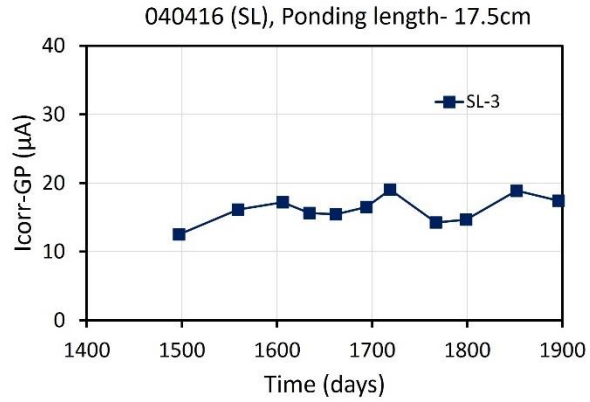

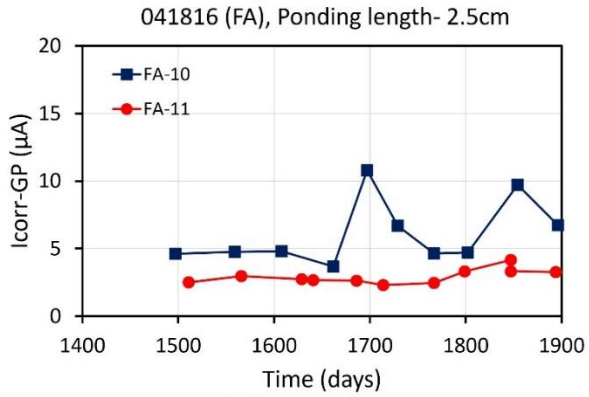

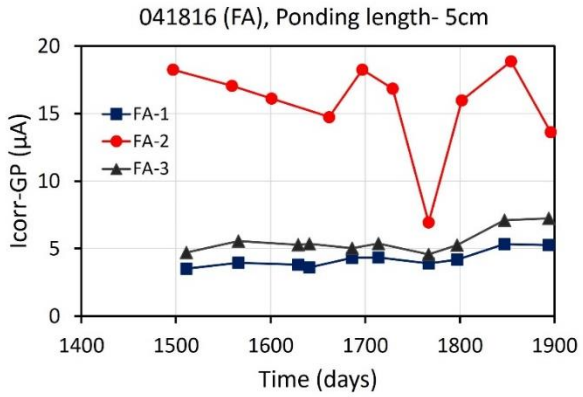

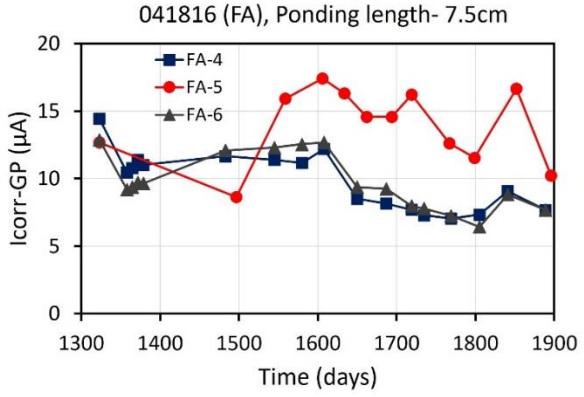

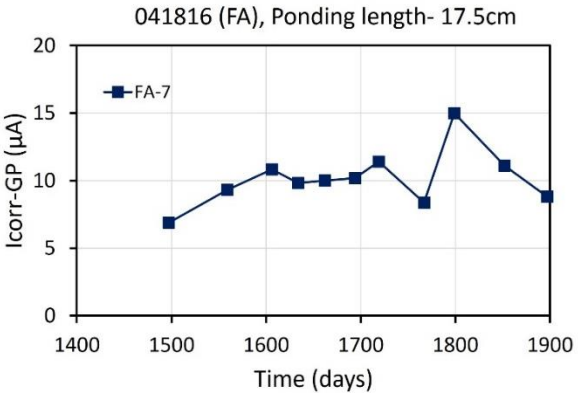

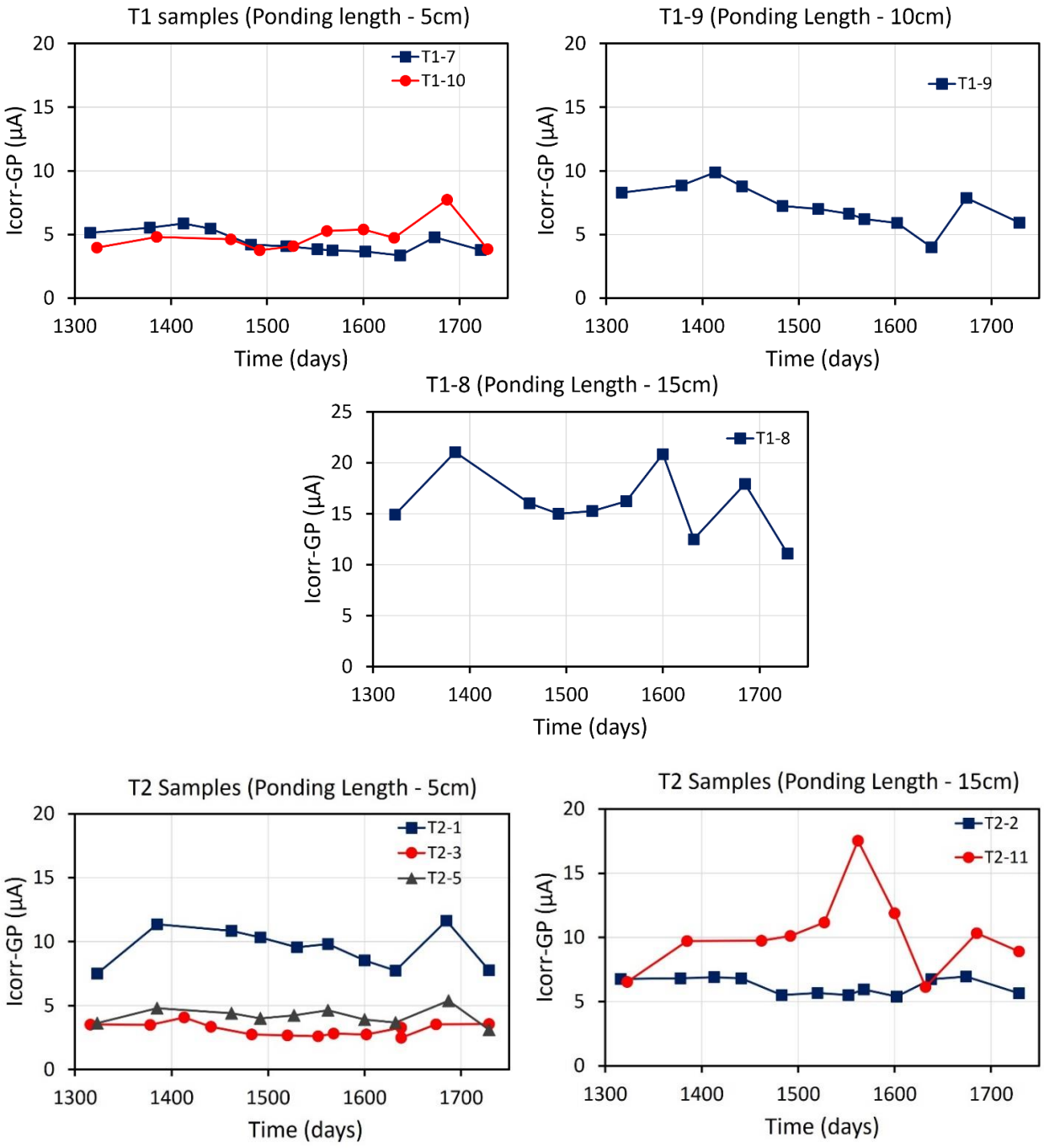

Figure 23. Icorr vs. time single rebar specimens

OCP vs. time

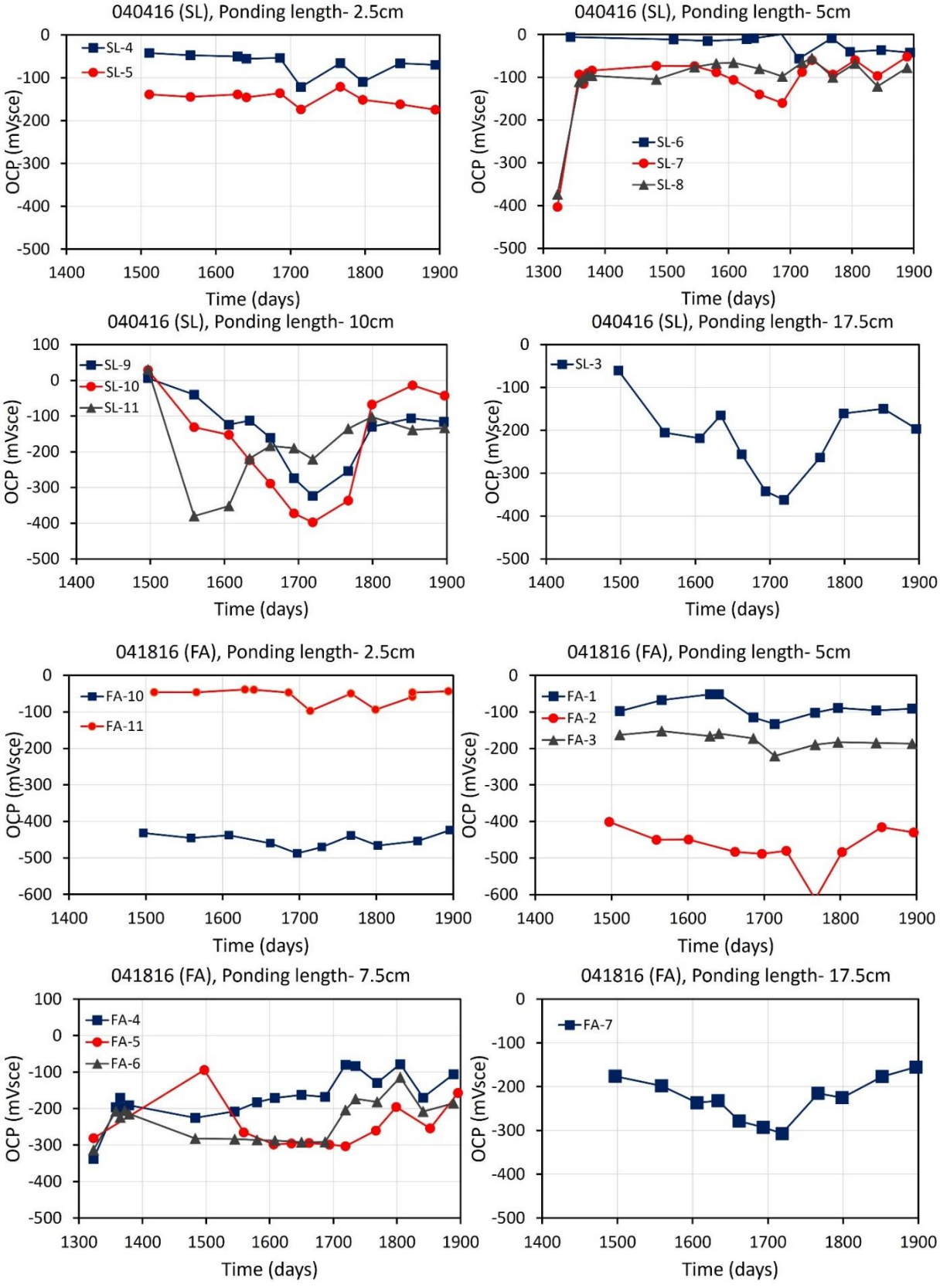
040416 (SL), Ponding length- 2.5cm
SL-4
SL-5
OCP (mVsce)
Time (days)
040416 (SL), Ponding length- 5cm
SL-6
SL-7
SL-8
OCP (mVsce)
Time (days)
040416 (SL), Ponding length- 10cm
SL-9
SL-10
SL-11
OCP (mVsce)
Time (days)
040416 (SL), Ponding length- 17.5cm
SL-3
OCP (mVsce)
Time (days)
041816 (FA), Ponding length- 2.5cm
FA-10
FA-11
OCP (mVsce)
Time (days)
041816 (FA), Ponding length- 5cm
FA-1
FA-2
FA-3
OCP (mVsce)
Time (days)
041816 (FA), Ponding length- 7.5cm
FA-4
FA-5
FA-6
OCP (mVsce)
Time (days)
041816 (FA), Ponding length- 17.5cm
FA-7
OCP (mVsce)
Time (days)

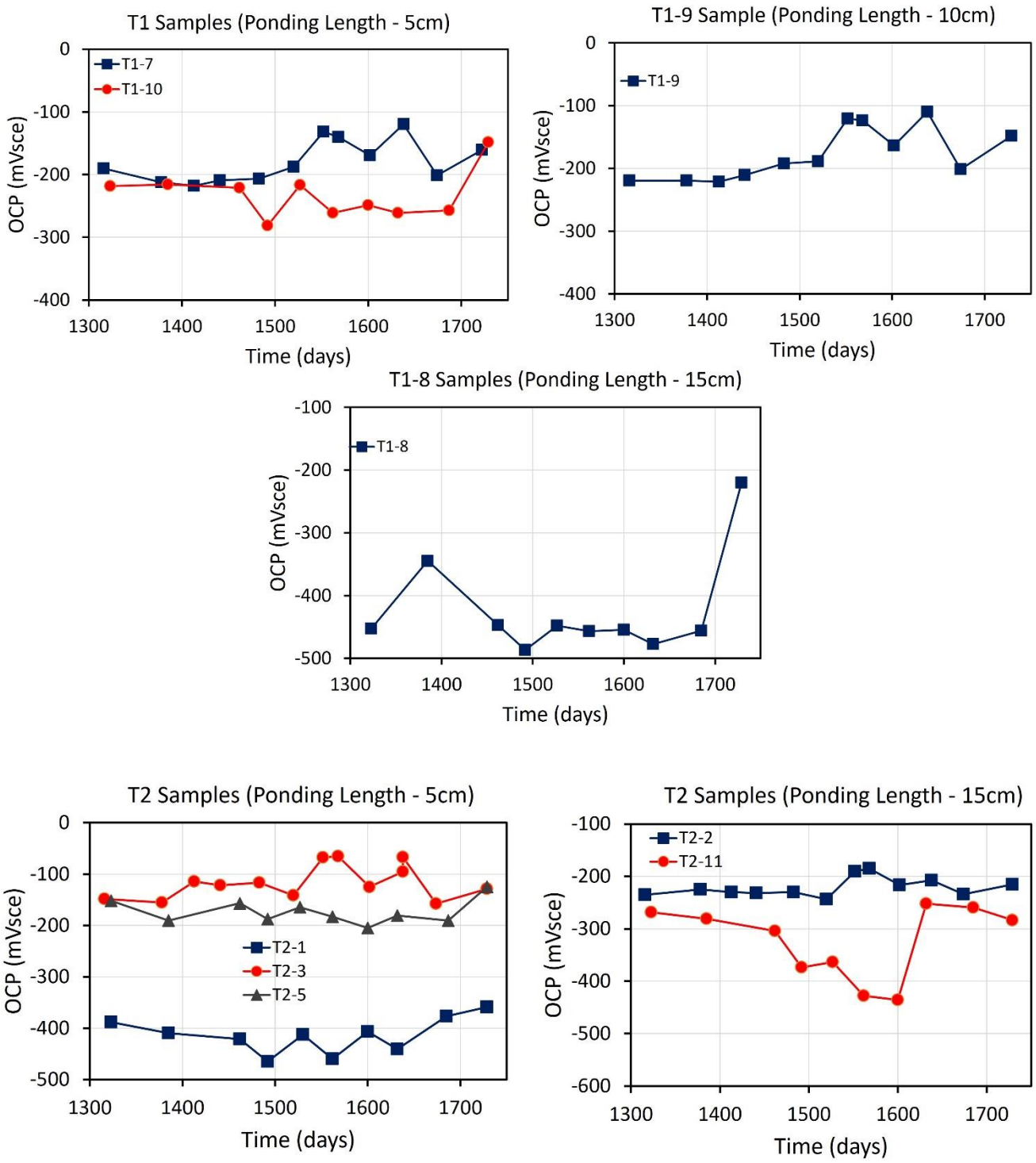

Figure 24. OCP vs. time single rebar specimens

Appendix C – Three Rebars samples:

Icorr vs. time (reported period)

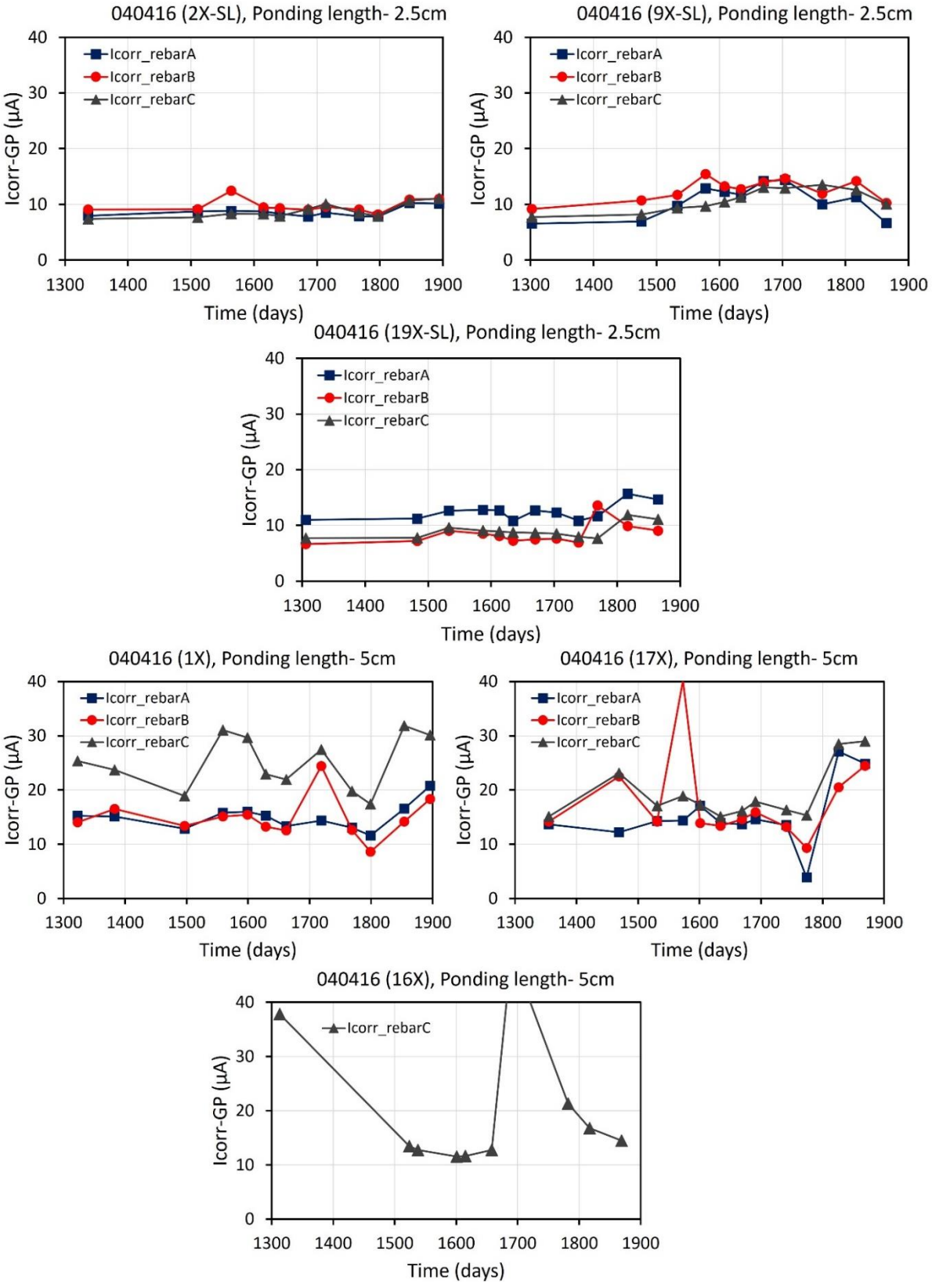

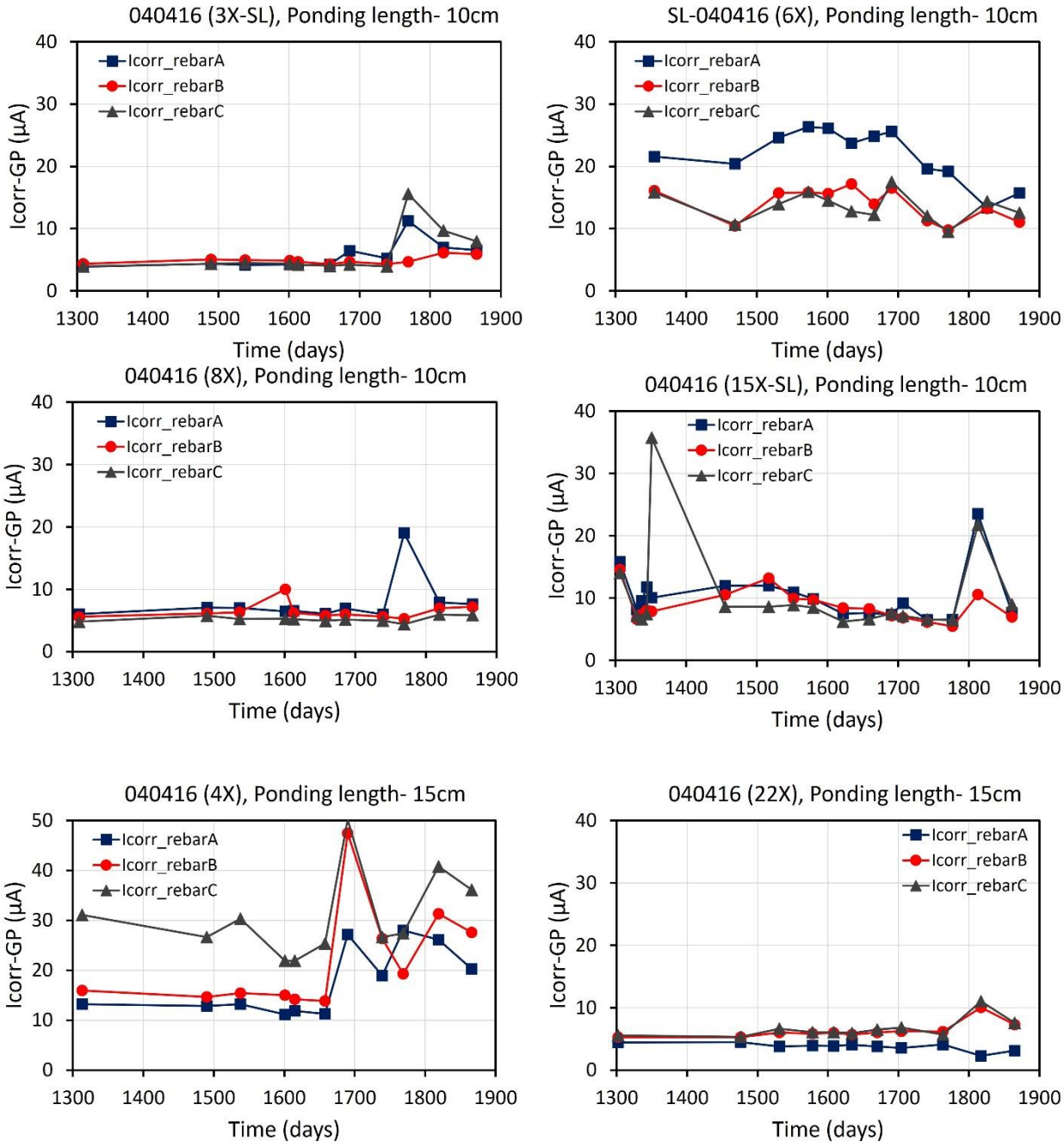

Figure 25. Icorr vs. time SL three rebar specimens

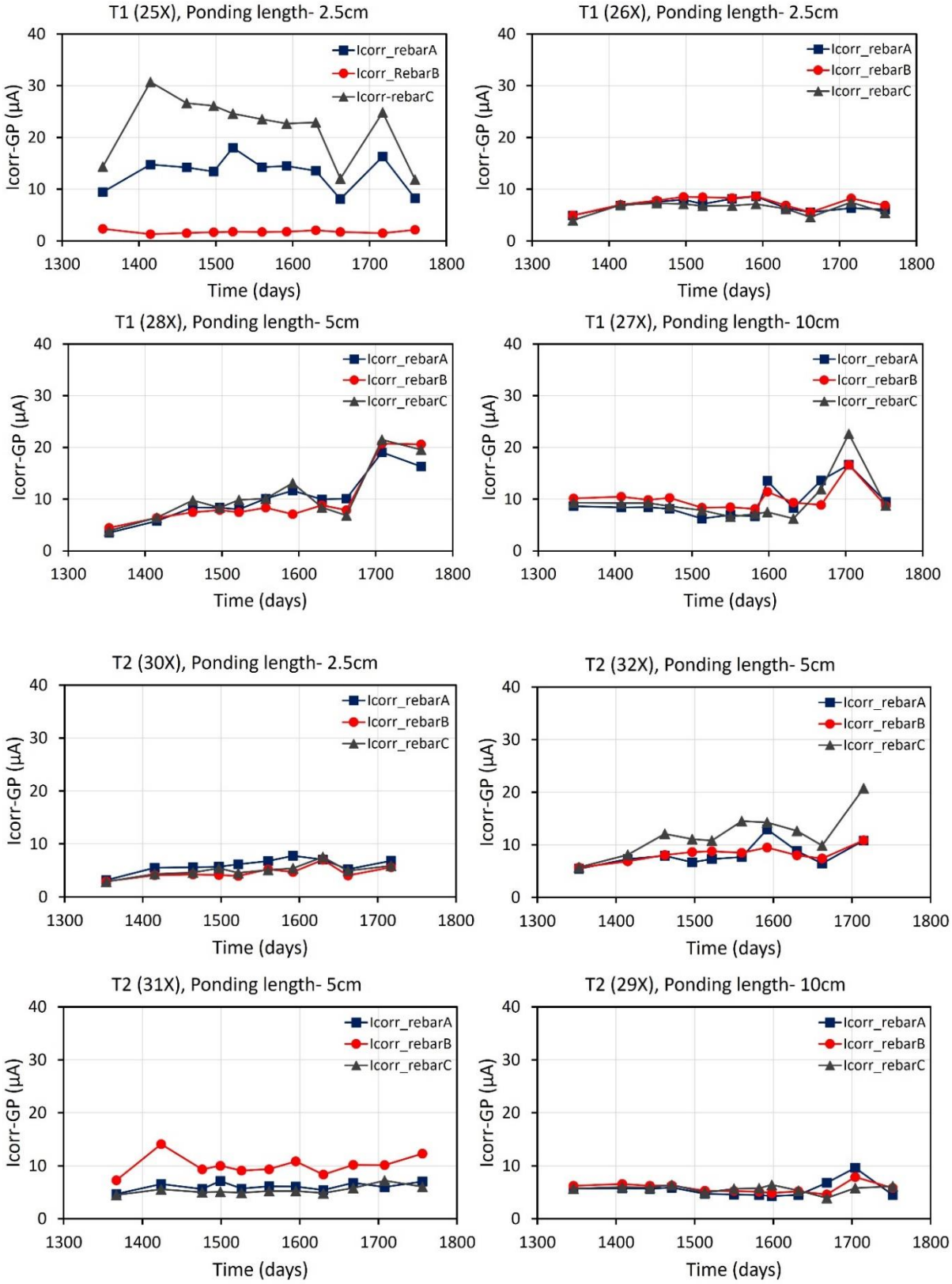

Figure 26. Icorr vs. time T1 and T2 three rebar specimens.

OCP vs. time (reported period)

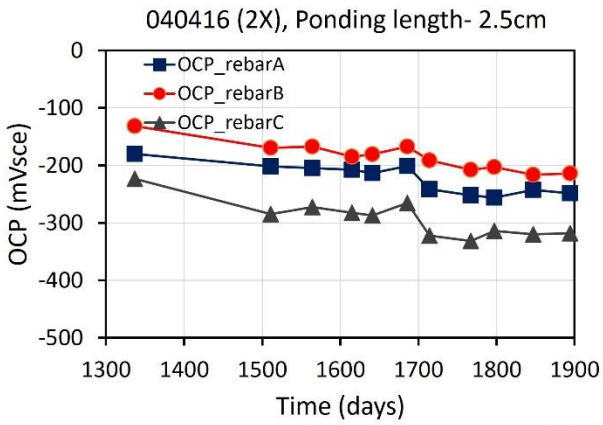

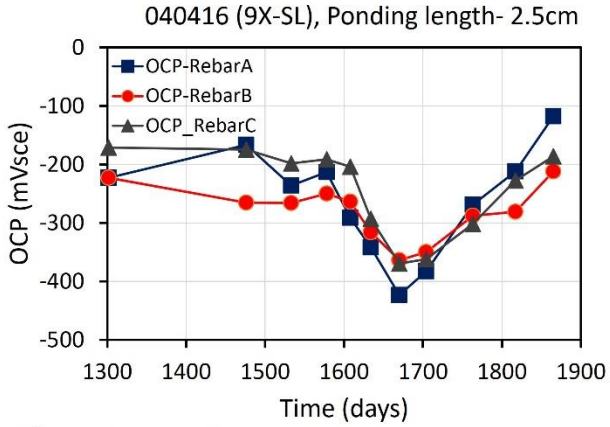

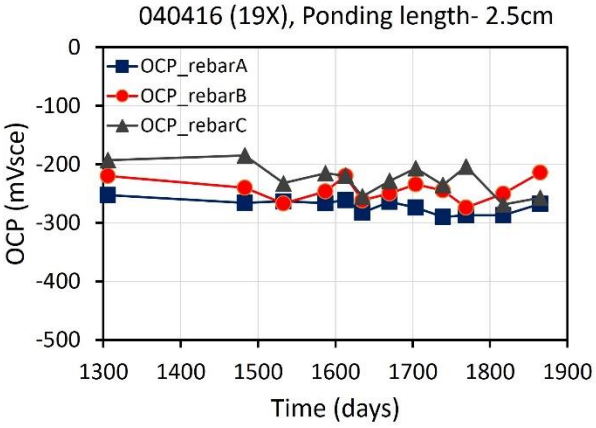

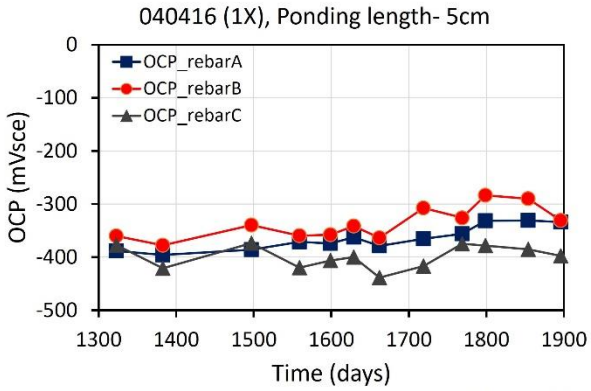

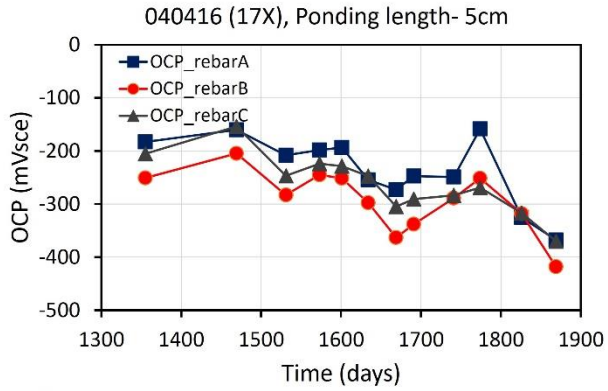

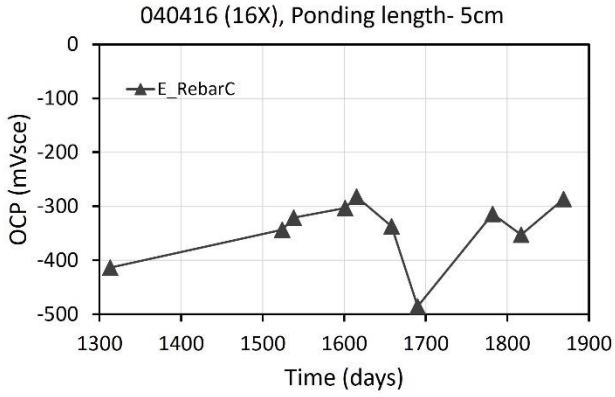

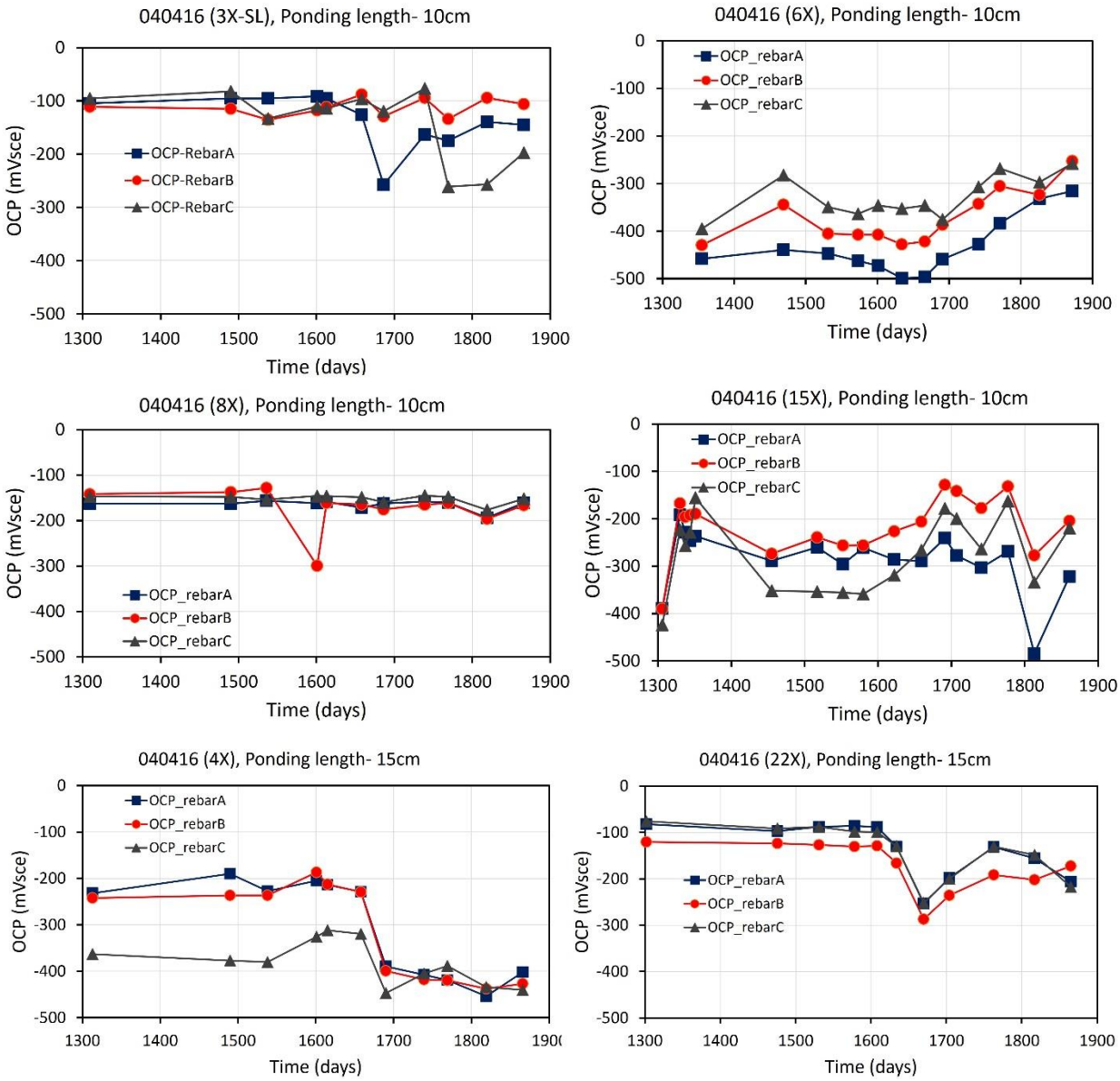

Figure 27. OCP vs. time, SL three rebar specimens

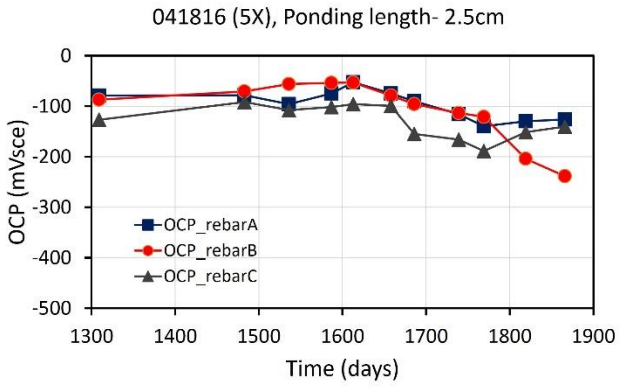
041816 (5X), Ponding length- 2.5cm
OCP (mVsce)
Time (days)
OCP_rebarA
OCP_rebarB
OCP_rebarC

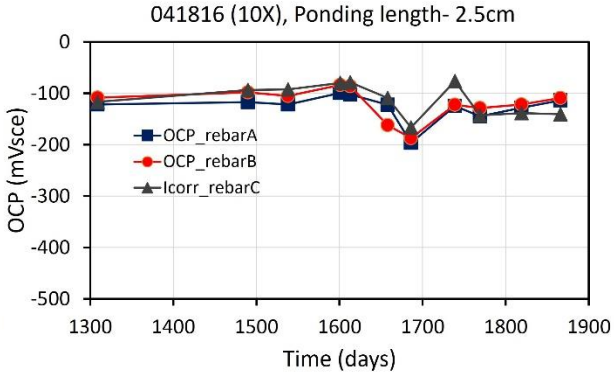
041816 (10X), Ponding length- 2.5cm
OCP (mVsce)
Time (days)
OCP_rebarA
OCP_rebarB
Icorr_rebarC

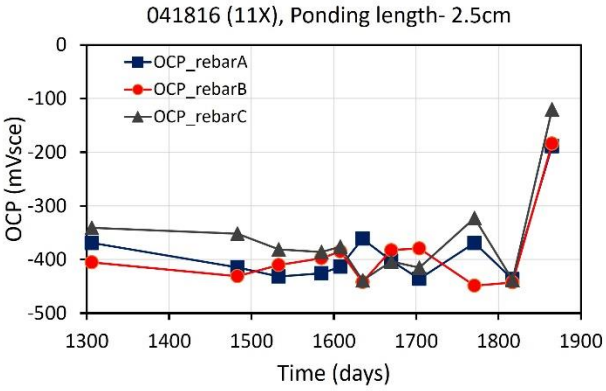
041816 (11X), Ponding length- 2.5cm
OCP (mVsce)
Time (days)
OCP_rebarA
OCP_rebarB
OCP_rebarC

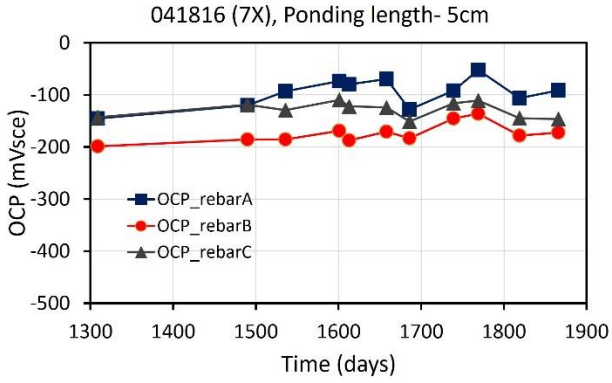
041816 (7X), Ponding length- 5cm
OCP (mVsce)
Time (days)
OCP_rebarA
OCP_rebarB
OCP_rebarC

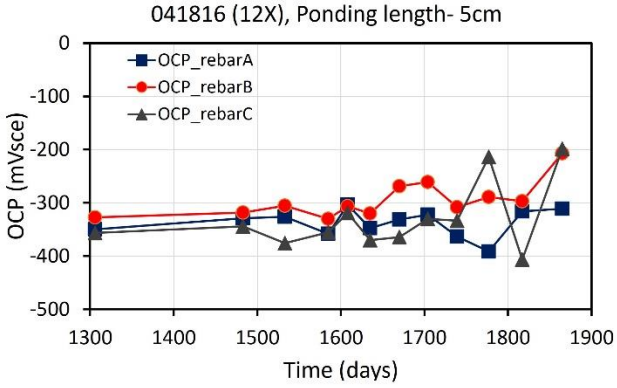
041816 (12X), Ponding length- 5cm
OCP (mVsce)
Time (days)
OCP_rebarA
OCP_rebarB
OCP_rebarC

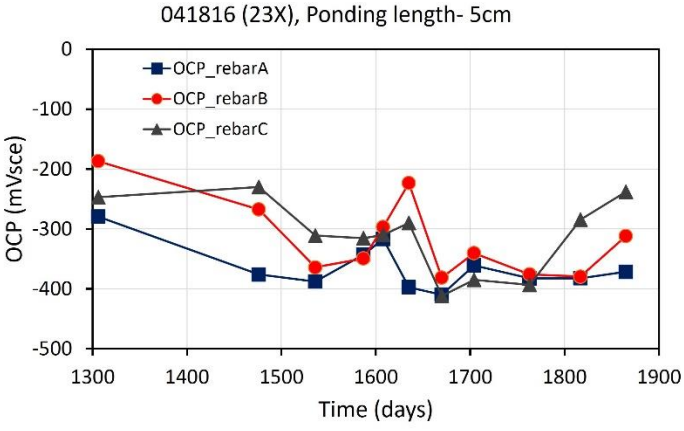
041816 (23X), Ponding length- 5cm
OCP (mVsce)
Time (days)
OCP_rebarA
OCP_rebarB
OCP_rebarC

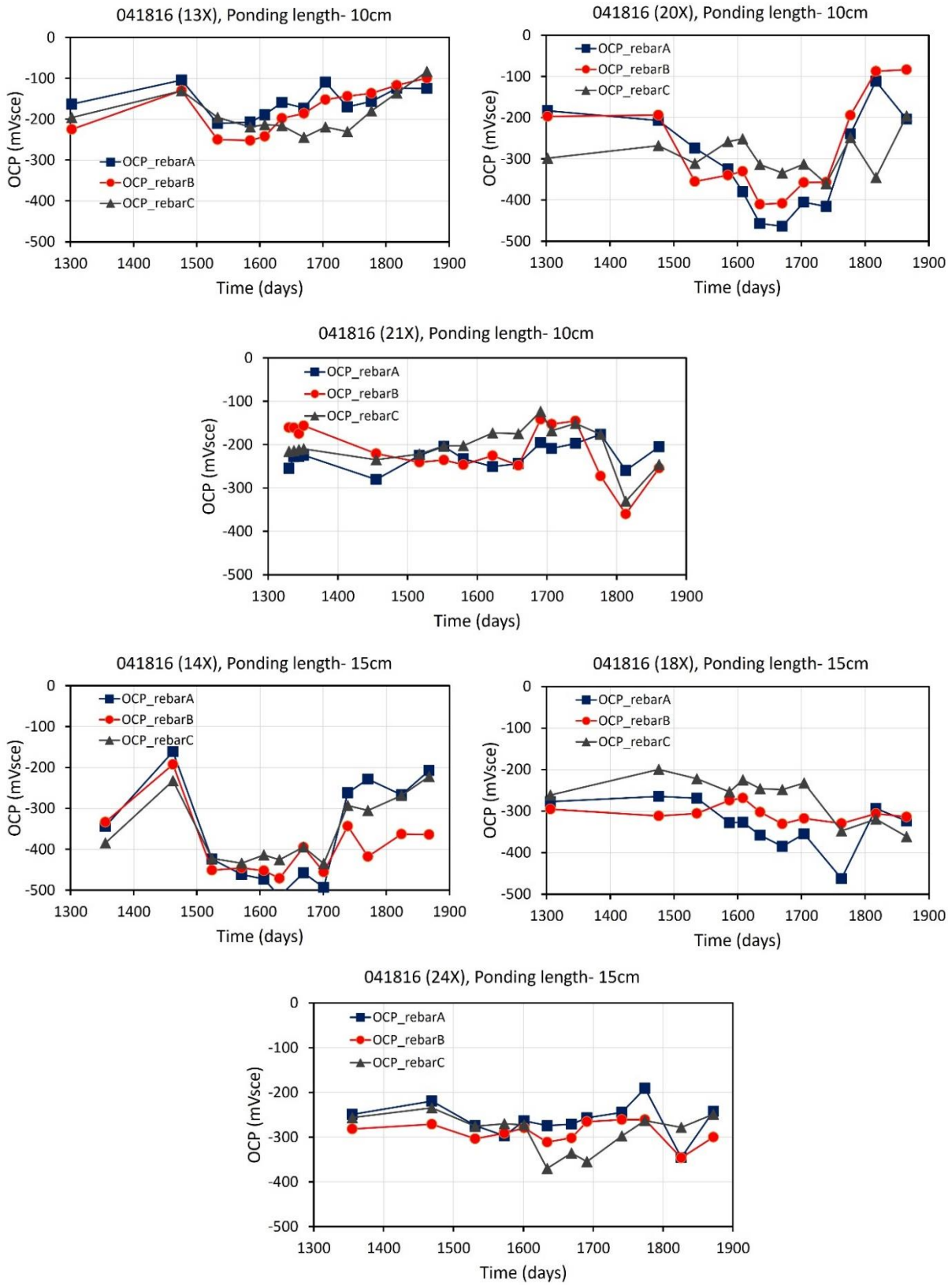

Figure 28. OCP vs. time, FA three rebar specimens

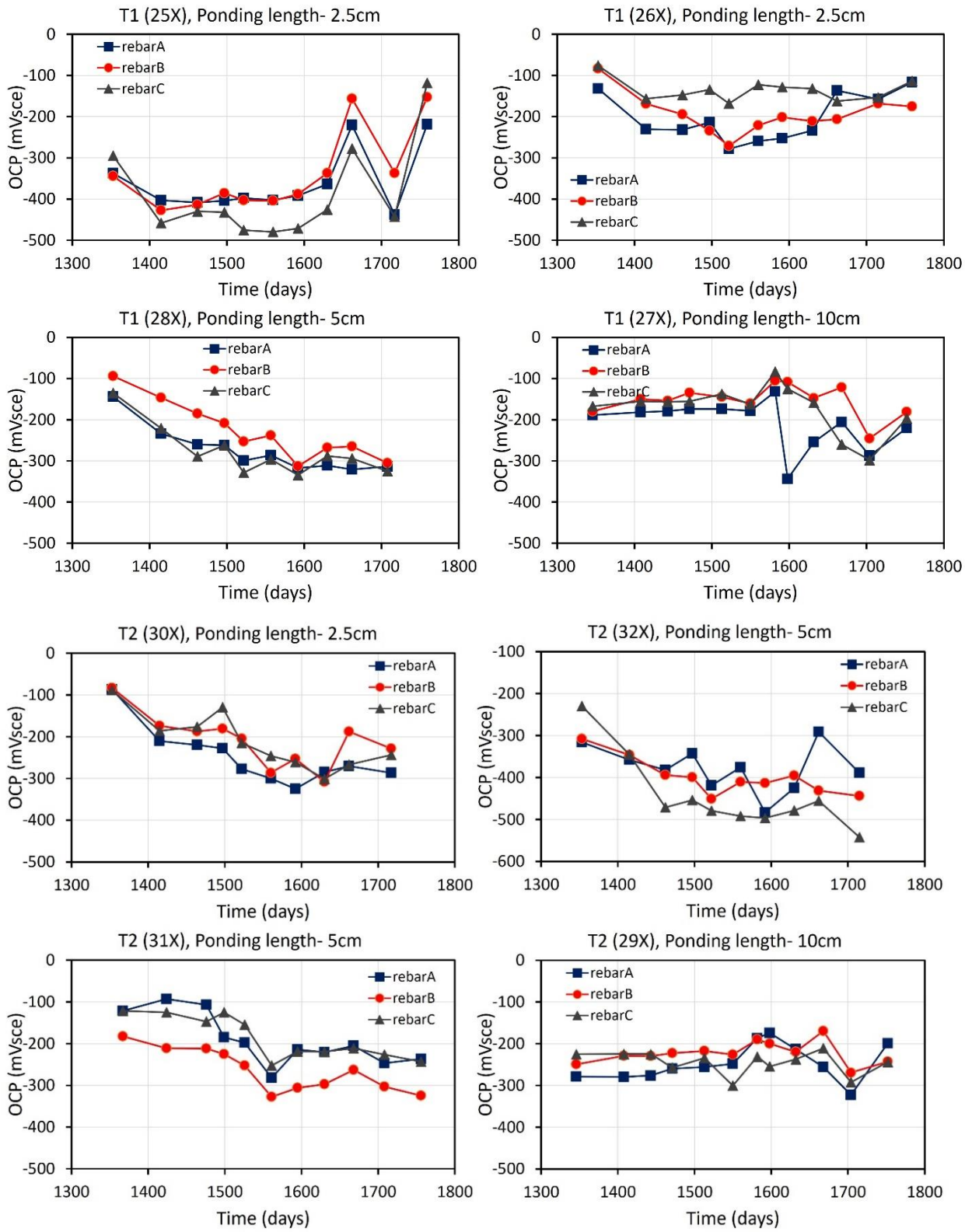

Figure 29. OCP vs. time, T1 and T2 three rebar specimens